HHS Public Access

Author manuscript

Cell Rep. Author manuscript; available in PMC 2023 December 19.

Published in final edited form as:

Cell Rep. 2023 November 28; 42(11): 113214. doi:10.1016/j.celrep.2023.113214.

LPGAT1 controls MEGDEL syndrome by coupling phosphatidylglycerol remodeling with mitochondrial transport

Haoran Sun[1,3], **Jun Zhang**[2,3], **Qianqian Ye**[1,2], **Ting Jiang**[1], **Xueling Liu**[1], **Xiaoyang Zhang**[1], **Fanyu Zeng**[1,2], **Jie Li**[1], **Yue Zheng**[1], **Xianlin Han**[2], **Chuan Su**[1], **Yuguang Shi**[2,4,*]

[1]Department of Biochemistry and Molecular Biology, Nanjing Medical University, Nanjing, 101 Longmian Avenue, Nanjing, Jiangsu Province 211166, China

[2]Sam and Ann Barshop Institute for Longevity and Aging Studies, Department of Pharmacology, University of Texas Health Science Center at San Antonio, 4939 Charles Katz Drive, San Antonio, TX 78229, USA

[3]These authors contributed equally

[4]Lead contact

SUMMARY

Phosphatidylglycerol (PG) is a mitochondrial phospholipid required for mitochondrial cristae structure and cardiolipin synthesis. PG must be remodeled to its mature form at the endoplasmic reticulum (ER) after mitochondrial biosynthesis to achieve its biological functions. Defective PG remodeling causes MEGDEL (non-alcohol fatty liver disease and 3-methylglutaconic aciduria with deafness, encephalopathy, and Leigh-like) syndrome through poorly defined mechanisms. Here, we identify LPGAT1, an acyltransferase that catalyzes PG remodeling, as a candidate gene for MEGDEL syndrome. We show that PG remodeling by LPGAT1 at the ER is closely coordinated with mitochondrial transport through interaction with the prohibitin/TIMM14 mitochondrial import motor. Accordingly, ablation of LPGAT1 or TIMM14 not only causes aberrant fatty acyl compositions but also ER retention of newly remodeled PG, leading to profound loss in mitochondrial crista structure and respiration. Consequently, genetic deletion of the *LPGAT1* in mice leads to cardinal features of MEGDEL syndrome, including 3-methylglutaconic aciduria, deafness, dilated cardiomyopathy, and premature death, which are highly reminiscent of those caused by *TIMM14* mutations in humans.

In brief

*Correspondence: shiy4@uthscsa.edu.

AUTHOR CONTRIBUTIONS

Conceptualization, Y.S.; methodology, Y.S., H.S., and J.Z.; investigation, H.S., J.Z., Q.Y., X.L., X.Z., J.L., Y.Z., and F.Z.; formal analysis, H.S., J.Z., Q.Y., X.L., and X.Z.; writing – original draft, Y.S., J.Z., and H.S.; writing – review & editing, Y.S., J.Z., and H.S.; funding acquisition, Y.S. and J.Z.; supervision, Y.S., C.S., and X.H.

DECLARATION OF INTERESTS

The authors declare no competing interests.

SUPPLEMENTAL INFORMATION

Supplemental information can be found online at https://doi.org/10.1016/j.celrep.2023.113214.

Phosphatidylglycerol is a mitochondrial phospholipid but is remodeled in the ER. Little is known about how the remodeled phosphatidylglycerol is transported back to mitochondria. Sun et al. demonstrate that phosphatidylglycerol remodeling by LPGAT1 closely coordinates with the mitochondrial PHB/TIM translocon and that ablation of LPGAT1 or disruption of the coordination process causes MEGDEL syndrome.

Graphical Abstract

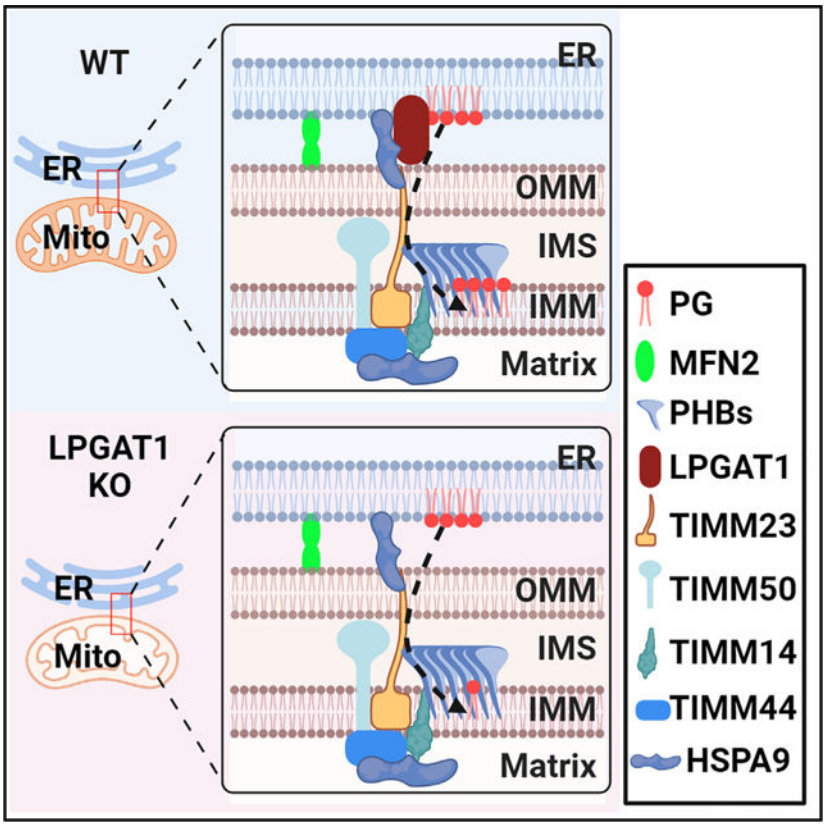

INTRODUCTION

Phosphatidylglycerol (PG) is a minor mitochondrial glycerophospholipid required for the synthesis of cardiolipin (CL).[1] In the inner mitochondrial membrane, cytidine diphosphate diacylglycerol (CDP)-diacylglycerol synthase catalyzes the conversion of phosphatidic acid into CDP-diacylglycerol, which is then converted to PG phosphate by the phosphatidyl glycerophosphate synthase 1 by transferring a phosphatidyl group to the glycerol-3-phosphate. The PG phosphate is then catalyzed by phosphatidyl glycerophosphate phosphatase to form PG. Finally, CL synthase 1 catalyzes the formation of immature CL by using CDP-diacylglycerol and PG as substrates.[2–5] CL plays an important role in maintaining normal mitochondrial function, including membrane structure, dynamics, mitochondrial DNA (mtDNA) biogenesis, and mitophagy.[3,6–9] PG accounts for less than 1% of total phospholipids in most mammalian tissues, except for lung, where it represents about 5% of total phospholipids and is a major component of lung surfactant.[10,11] In contrast

to CL, little information is known about the functional importance of PG in mitochondria, although PG deficiency in yeast cells leads to mitochondrial dysfunction beyond those caused by CL depletion.[12,13]

PG is subjected to remodeling of its fatty acyl chains to achieve mature acyl compositions after its *de novo* biosynthesis in mitochondria, a metabolic process also known as the Lands cycle. The remodeling allows incorporation of appropriate acyl composition for its biological functions and to prevent the harmful effect of lysophosphatidylglycerol (LPG) accumulation.[1] Consequently, defective remodeling of PG is part of the pathophysiology associated with Barth syndrome (BTHS), which is characterized by dilated cardiomyopathy and premature death.[7,14–16] In addition, defective PG remodeling is implicated in the pathogenesis of non-alcohol fatty liver disease (NAFLD)[17,18] and 3-methylglutaconic (3-MGA) aciduria with deafness, encephalopathy, and Leigh-like (MEGDEL) syndrome,[19] an autosomal recessive disorder characterized by 3-MGA aciduria, psychomotor delay, muscle hypotonia, sensorineural deafness, and Leigh-like lesions in brain.[20] To date, all reported cases of MEGDEL syndrome are caused by mutations in the serine active site-containing protein 1 (*SERAC1*) gene, which is involved in PG remodeling at the mitochondrial associated membrane (MAM).[19] However, no transacylase or acyltransferase activity toward LPG has been identified from the SERAC1 protein to date, suggesting the presence of other MEGDEL candidate genes.

LPG acyltransferase 1 (LPGAT1) is an acyltransferase that catalyzes PG remodeling at MAM with LPG and acyl-CoA as substrates, as previously reported by us.[1] Our recent work demonstrates that PG remodeling by LPGAT1 also played an important role in attenuating mitochondrial dysfunction associated with NAFLD.[18] Target deletion of the *LPGAT1* gene caused defective PG remodeling and mitochondrial dysfunction, leading to the development of NAFLD.[18] In addition, LPGAT1 deficiency caused hepatopathy,[18] which is a cardinal feature of MEGDEL syndrome.[21] Moreover, a previous study indicated that the *LPGAT1* gene is mapped to a disease-causative genetic locus for dilated cardiomyopathy,[22] a common feature associated with BTHS and MEGDEL syndrome.[23–25] However, it remains elusive whether LPGAT1 regulates the onset of MEGDEL syndrome or dilated cardiomyopathy.

As a mitochondrial phospholipid, PG must be transported back to mitochondria after its remodeling at MAM, yet molecular mechanisms underlying the mitochondrial transport process remain poorly understood. In this study, we identified a pivotal role of LPGAT1 in regulating mitochondrial PG transport. In addition to its previously identified role in PG remodeling, we show that LPGAT1 specifically interacts with the prohibitin/transporter inner membrane (PHB-/TIM) complex, a mitochondrial import motor.[26] This interaction plays an important role in coupling PG remodeling at the MAM with mitochondrial import of newly remodeled PG. Using a lipid labeling technique recently developed by us,[27] we show that deletion of LPGAT1 or TIMM14, a component of the PHB/TIM complex, prevents mitochondrial transport of newly remodeled PG, resulting in a loss of mitochondrial cristae structure and respiration. Using mice with targeted deletion of LPGAT1, we further demonstrate that LPGAT1 deficiency causes defective PG remodeling and mitochondrial dysfunction similar to those caused by *TIMM14* mutations in humans, leading to the development of MEGDEL syndrome and dilated cardiomyopathy.[28]

RESULTS

Ablation of LPGAT1 causes dilated cardiomyopathy and premature death in mice

Using mice with a targeted deletion of the *LPGAT1* gene recently generated by us,[18] we investigated whether PG remodeling by LPGAT1 regulates the onset of MEGDEL syndrome. The results show that LPGAT1 deficiency significantly increased the incidence of generalized cyanosis and premature death within 24 h after birth in LPGAT1 knockout (KO) mice relative to the wild-type (WT) controls (Figure 1A). The survival rates of neonatal heterozygous and homozygous LPGAT1 KO mice declined to 85% and 56%, respectively (Figure S1A). LPGAT1 deficiency also caused lower birth weight (Figure S1B) and hypoglycemia (Figure S1C), leading to growth delay (Figure S1D). Furthermore, LPGAT1-deficient mice exhibited significantly higher mortality rates than the WT controls during adulthood due to the occurrence of sudden death, especially during the ages of 14–22 weeks (Figure 1B).

A previous study showed that the *LPGAT1* gene is localized at a genetic locus associated with dilated cardiomyopathy in humans.[22] We next investigated whether the low survival rate of LPGAT1 KO mice was caused by cardiac dysfunction, as some of the KO mice also exhibited sudden death. In support of this notion, we showed that ablation of LPGAT1 caused dilated cardiomyopathy, as evidenced by an increased heart weight-to-body weight ratio (Figures S1E and S1F) and an enlarged left ventricular (LV) internal diameter, which was analyzed by hematoxylin and eosin (H&E) staining of LV sections (Figure 1C). Consistent with the findings, LPGAT1 deficiency also led to bradycardia and LV dysfunction, as evidenced by decreased levels of heart rate (HR; Figure S1G), systolic blood pressure (Figure S1H), LV ejection fraction (EF; Figure 1D), and LV fractional shortening (FS; Figure 1E). LPGAT1 deficiency also significantly increased the LV internal diameter at end diastole and end systole (LVIDd and LVIDs, respectively; Figure 1F) without a significant effect on diastolic blood pressure (Figure S1I). Furthermore, ablation of LPGAT1 caused hypertrophy of cardiomyocytes, as demonstrated by the results from wheat germ agglutinin (WGA) staining of the LV sections (Figure 1G, quantified in Figure 1H). Consistent with the findings, LPGAT1 deficiency also significantly increased mRNA expression levels of key biomarkers associated with cardiac hypertrophy, including atrial natriuretic factor (*Anf*), brain natriuretic peptide (*Bnp*), β-myosin heavy chain (*β-Mhc*), and skeletal muscle α-actin (*Acta1*), as demonstrated by results from quantitative real-time PCR analysis (Figure 1I). Moreover, LPGAT1 deficiency caused excessive accumulation of collagen fibers in the heart, which is supported by results from both Masson's trichrome staining and Sirius red staining of LV sections (Figure 1J, quantified in Figure 1K, arrows highlight the fibrosis). Consistent with the findings, ablation of LPGAT1 also significantly increased the mRNA expression of key biomarkers of fibrosis, including collagen I (*Col 1*) and *Col III* in the LV of the KO mice (Figure 1L).

LPGAT1 deficiency leads to hearing loss, a common feature of MEGDEL syndrome

In addition to dilated cardiomyopathy,[29,30] MEGDEL syndrome often causes hearing loss.[31] To determine a role of LPGAT1 in regulating auditory function, we next examined the auditory function of WT control and LPGAT1 KO mice by using the auditory brainstem

response (ABR) test. Sound-evoked ABR recordings reflect synchronous activation of elements of the brainstem auditory pathway.[32] Indeed, LPGAT1 deficiency significantly increased the ABR threshold in all testing frequencies from 4 to 32 kHz, as shown by the representative ABR waveform recordings (Figures 2A and 2B) and the statistical analysis of the ABR threshold (Figure 2C), revealing a severe hearing deficit in LPGAT1-deficient mice. Moreover, LPGAT1 deficiency caused apoptosis, inflammation, and oxidative stress in the cochlear, which is supported by increased mRNA levels of caspase-3 (*Casp3*), allograft inflammatory factor 1 (*Aif-1*), interleukin-1β (*IL-1β*), NADPH oxidase 4 (*Nox-4*), and thioredoxin reductase (*Txnrd*), as determined by the quantitative real-time PCR analysis (Figure 2D).

LPGAT1 deficiency causes 3-MGA aciduria and liver damage, signature defects in MEGDEL syndrome

Another common feature of MEGDEL syndrome is the presence of high levels of 3-MGA in urine.[30] We next determined the 3-MGA level in the urine of WT and LPGAT1 KO mice. The data showed that the 3-MGA level in the urine was strikingly elevated in LPGAT1 KO mice relative to WT control mice (Figure S2A). Consistent with our previous data, which showed that LPGAT1 deficiency caused hepatopathy in mice,[18] LPGAT1 deficiency significantly increased serum level of alanine aminotransferase (ALT), aspartate aminotransferase (AST), and total bilirubin (TBIL) (Figures S2B–S2D). Moreover, the blood ammonia and urea nitrogen (BUN) levels were also significantly elevated in LPGAT1 KO mice (Figures S2E and S2F), further supporting the notion that ablation of LPGAT1 caused liver damage. Consistent with hypoglycemia, LPGAT1 deficiency significantly increased serum levels of lactic acid (LD), pyruvate, and total ketone bodies (Figures S2G–S2I), implicating increased levels of gluconeogenesis as a consequence of hypoglycemia.

Ablation of LPGAT1 diminishes mitochondrial cristae structure and respiration

PG plays a pivotal role in supporting mitochondrial membrane curvature, cristae structure, and respiration.[13,33] The metabolic defects in LPGAT1 KO mice promoted us to determine whether defective PG remodeling damages mitochondrial morphology and function. Using primary mouse embryonic fibroblasts (MEFs), we first determined the effect of LPGAT1 deficiency on mitochondrial morphology by electronic microscopy (EM) analysis. As shown in Figure 3A, LPGAT1 deficiency led to abnormal mitochondrial ultrastructure, as revealed by a significant loss of mitochondrial cristae structure in MEFs from LPGAT1 KO mice (Figure 3A). Mitochondrial cristae structure plays a pivotal role in supporting oxidative phosphorylation and mtDNA biogenesis.[34,35] Consistent with defective mitochondrial cristae morphology, LPGAT1 deficiency caused a significant decrease in both mtDNA copy number (Figure 3B) and mitochondrial membrane potential (Figure 3C), leading to severe oxidative stress and elevated levels of reactive oxygen species (ROS) (Figure 3D). Using the Seahorse flux analyzer, we next analyzed the effect of LPGAT1 on mitochondrial respiration by measuring changes in oxygen consumption rate (OCR) in primary MEFs. The results showed that LPGAT1 deficiency significantly impaired mitochondrial respiration, as evidenced by decreased levels of basal, maximal, and ATP-linked OCRs in the LPGAT1-deficient MEFs relative to WT controls (Figure 3E, quantified in Figure 3F).

LPGAT1 specifically interacts with the PHB/TIM complex, which requires integrity of MAM

As a mitochondrial phospholipid, PG must be transported from the MAM to mitochondria after remodeling by LPGAT1.[36,37] However, little information is known about the trafficking process. The stomatin/PHB/flotillin/HflK/C (SPFH) family of proteins is commonly believed to regulate the lateral distribution of both membrane lipids and proteins by forming a mitochondrial importer complex.[38] Interestingly, a previous study showed that TIMM14, also known as DNAJC19, forms a complex with PHB to regulate CL remodeling.[30] TIMM14, a homolog of yeast Pam18/Tim14, is also a component of the mitochondrial protein import machinery in the inner mitochondrial membrane. Mutation in TIMM14 causes dilated cardiomyopathy with ataxia (DCMA)[28] and 3-MGA aciduria,[30,39] seminal features of MEGDEL syndrome, which prompted us to investigate whether LPGAT1 coordinates with the PHB/TIM complex to couple PG remodeling with mitochondrial transport of newly remodeled PG. Using FLAG-LPGAT1 as the “bait,” we carried out co-immunoprecipitation (coIP) analysis in HEK293T to determine whether LPGAT1 specifically interacts with the PHB/TIMM14 complex. Remarkably, LPGAT1 specifically interacted with multiple members of the endogenous TIMM23 translocon, including TIMM14, TIMM23, TIMM44, and TIMM50. LPGAT1 also interacted with multiple components of the PHB complex, including PHB1, PHB2 and the m-AAA protease AFG3L2 (Figure 4A), implicating a key role of the PHB/TIM complex in mitochondrial transport of newly remodeled PG. Moreover, LPGAT1 also specifically interacts with heat shock protein family A member 9 (HSPA9), a member of heat shock protein 70. In addition to mitochondria, HSPA9 protein was abundantly found in the ER,[40] implicating a potential role for HSPA9 in tethering LPGAT1 with the TIMM23 translocon.

Although the PHB/TIM complex is commonly believed to mediate protein trafficking of the inner mitochondrial membrane, its involvement in mitochondrial phospholipid import remains elusive.[38,41] Additionally, the PHB/TIM complex is commonly believed to be localized in the inner mitochondrial membrane, raising an intriguing question about how LPGAT interacts with the complex, as our previous work showed that LPGAT1 is primarily located at the MAM.[1,18] The MAM plays a key role in non-vesicular lipid trafficking between the ER and mitochondria.[42] We reasoned whether the MAM could also bridge the gap of the interaction of LPGAT1 with the PHB/TIM complex. We tested this hypothesis by first determining whether LPGAT1 specifically interacts with mitofusin 2 (MFN2), which plays a key role in maintaining the integrity of the MAM by tethering the ER with mitochondria.[43] Indeed, we found that LPGAT1 specifically interacted with MFN2, as shown by results from coIP analysis in HEK293T cells (Figure 4C). Consistent with the findings, small interfering RNA (siRNA)-mediated knockdown of MFN2 significantly attenuated the interaction between LPGAT1 and PHB/TIM complex proteins (Figure 4C), implying that MFN2 could also serve as a tether for the interaction of LPGAT1 with the PHB/TIM complex. In support of this notion, STRING (https://string-db.org/) analysis showed that MFN2 forms a comprehensive interactome with PHB/TIM proteins (Figure 4B).

LPGAT1 coordinates with TIMM14 to facilitate mitochondrial trafficking of newly remodeled PG

The association of LPGAT1 with the PHB/TIM complex prompted us to determine whether the interaction is required for mitochondrial import of newly remodeled PG. To test the hypothesis, we determined whether deletion of either LPGAT1 or TIMM14 would impair mitochondrial transport of newly remodeled PG in live C2C12 cells by using the *de novo* phospholipid labeling method recently developed by us.[27] LPGAT1 KO cells or vector controls were stained with MitoTracker Red to label mitochondria and were cultured briefly in the presence or the absence of LPG and nitro-benzoxadiazolyl (NBD)-acyl-CoA, which were used as substrates for PG remodeling by the endogenous enzymes. Attachment of NBD to newly remodeled PG allows us to monitor the mitochondrial trafficking of newly remodeled PG by confocal imaging analysis in live cells. As previously reported by us, newly remodeled PG was rapidly transported from the ER to mitochondria in vector control cells, as evidenced by the co-localization of NBD-PG (green) with mitochondria (red) (Figure 5A, arrows highlight the co-localization of NBD-PG with mitochondria in yellow). In contrast, LPGAT1 deficiency significantly attenuated mitochondrial transport of newly remodeled PG in LPGAT1 KO cells (Figure 5B). Likewise, LPGAT1 deficiency in primary hepatocytes isolated from LPGAT1 KO mice also significantly impaired mitochondrial PG transport (Figure S3, arrows highlight the co-localization of NBD-PG with mitochondria). Remarkably, ablation of the TIMM14 by CRISPR-Cas9 technique (Figure S6A) also significantly attenuated mitochondrial transport of newly remodeled PG (Figure 5C). In contrast, neither LPGAT1 nor TIMM14 was required for mitochondrial transport of other newly remodeled phospholipids, including CL, phosphatidylethanolamine (PE), and phosphatidylcholine (PC), as demonstrated by results from confocal imaging analysis of LPGAT1 KO (Figure S4) and TIMM14 KO cells (Figure S5).

To scrutinize the specificity of LPGAT1's interaction with TIMM14 in mediating mitochondrial PG transport, we next determined whether ablation of LPGAT1 or TIMM14 in C2C12 cells would also lead to the ER retention of newly remodeled PG. To do so, C2C12 cells transiently transfected with Mito-BFP and dsRed2-ER5 to label mitochondria and the ER, respectively, were cultured in the presence or the absence of LPG and NBD-CoA and analyzed for co-localization of newly remodeled PG with the ER or mitochondria by confocal imaging analysis. In further support of the notion that LPGAT1 coordinates with the PHB/TIM complex to promote mitochondrial PG trafficking, ablation of either LPGAT1 or TIMM14 leads to the ER retention of newly remodeled PG (Figures 6A–6C, PG/ER panel, arrows highlight the co-localization of NBD-PG with the ER in yellow). Consequently, depletion of either LPGAT1 or TIMM14 dramatically reduced mitochondrial content of newly remodeled PG and the ratio of mitochondrial PG to total cellular PG (Figures 6D and 6E). Consistent with the important role of PG in supporting mitochondrial morphology and respiration, TIMM14 deficiency also caused multiple metabolic defects that are highly reminiscent of those caused by LPGAT1 deficiency, including decreased mitochondrial membrane potential (Figure S6B) and increased ROS production (Figure S6C), leading to a significant loss of mitochondrial cristae structure (Figure S6D). TIMM14 deficiency also significantly impaired mitochondrial respiration, as evidenced by decreased

levels of basal, maximal, and ATP-linked OCRs as well as the respiratory spare capacity from Seahorse flux analysis (Figure S6E, quantified in Figure S6F).

To further scrutinize the specificity of LPGAT1's interaction with TIMM14 in mediating mitochondrial PG transport, we next determine whether MAM integrity is also required for mitochondrial transport of newly remodeled PG, as MFN2 deficiency abolished the interaction of LPGAT1 with the PHB/TIM complex. To do so, we generated C2C12 cells with target deletion of MFN2 by using the CRISPR–Cas9 technique. The KO of MFN2 was confirmed by western blot analysis (Figure 6G). Consistent with the findings that MAM integrity is required for the interaction of LPGAT1 with the PHB/TIM complex, ablation of MFN2 also significantly impaired the mitochondrial PG transport, as shown by the results from confocal imaging analysis (Figure 6F, quantified in Figures 6H and 6I, arrows highlight the co-localization of NBD-PG with mitochondria in yellow). Together, these findings further confirmed that LPGAT1 coordinates with the PHB/TIM complex to facilitate mitochondrial transport of newly remodeled PG, which depends on the integrity of MAM.

Ablation of LPGAT1 leads to aberrant PG and CL acyl compositions similar to those caused by TIMM14 deficiency

A previous report showed that an elevated PG-34:1/PG-36:1 ratio is a major defect associated with MEGDEL syndrome caused by *SERAC1* mutations.[19] The remarkable functional similarities between LPGAT1 and TIMM14 in regulating mitochondrial morphology, function, and PG transport prompted us to investigate whether the LPGAT1/TIMM14 interaction plays an important role in regulating PG acyl compositions by lipidomic analysis. Remarkably, ablation of TIMM14 caused similar changes in acyl compositions of PG as in LPGAT1-deficient cells, including increased abundance of PG species with very long and polyunsaturated fatty acyl chains, such as those with 8–12 double bonds (Figures 7A–7D). Likewise, TIMM14 deficiency also caused significant changes in the acyl profile of individual PG species similar to that caused by LPGAT1 deficiency (Figures S7A and S7B). In support of LPGAT1 as a candidate gene for MEGDEL syndrome, LPGAT1 deficiency also significantly increased the ratio of PG-34:1/PG-36:1 relative to vector control cells, which is a major defect associated with MEGDEL syndrome caused by *SERAC1* gene mutation[19] (Figures S8A–S8C).

PG is a precursor for the synthesis of CL. We next determined the effect of LPGAT1 and TIMM14 deficiencies on CL acyl compositions in cells deficient in LPGAT1 or TIMM14 expression by lipidomic analysis. In final support of the functional importance of the LPGAT1/TIMM14 interaction, LPGAT1 deficiency caused remarkable changes in CL acyl compositions similar to those caused by TIMM14 deficiency, including a significant decrease in CL species with 68 carbons concurrently with increased abundance of CL species with 72–74 carbons (Figures 7E and 7G). Likewise, both LPGAT1 and TIMM14 deficiencies significantly increased the unsaturation of CL, as evidenced by increased abundance of CL species with more than 6 double bonds (Figures 7F and 7H). Consistently, LPGAT1 KO cells also share remarkable acyl profiles of individual CL species with that of the TIMM14 KO cells (Figures S9A and S9B). However, there were also major differences

between LPGAT1 and TIMM14 in regulating CL acyl compositions. As such, LPGAT1 deficiency caused opposite changes to TIMM14 deficiency in the abundance of CL species with 70 carbons with 3 double bonds (Figures 7F and 7H), suggesting that TIMM14 is likely involved in mitochondrial transport of newly remodeled CL from other remodeling pathways.

DISCUSSION

PG plays a pivotal role in supporting mitochondrial function as a substrate for CL synthesis. However, circumstantial evidence from yeast studies suggests that PG also possesses biological functions beyond those of CL.[12,13] Accordingly, defective PG remodeling leads to rare but more severe forms of genetic disorders in humans, such as MEGDEL syndrome, than those caused by defective CL remodeling.[23–25] Currently, the most well-studied cases of MEGDEL syndrome are associated with mutations in the *SERAC1* gene, which is implicated in the remodeling of PG, although no LPG acyltransferase activity has been identified from SERAC1 to date.[19] It remains debatable whether there are other genetic causes of MEGDEL syndrome. In this study, we identified the *LPGAT1* gene as a candidate gene for MEGDEL syndrome, which is supported by multiple lines of evidence. Accordingly, we show that ablation of LPGAT1 in mice leads to multiple common features of MEGDEL syndrome, including neonatal hypoglycemia, high mortality rate, sudden death, growth delay, 3-MGA aciduria, deafness, hepatopathy, and dilated cardiomyopathy. LPGAT1 deficiency also caused defective remodeling of PG with aberrant fatty acyl compositions that were commonly found in patients with MEGDEL syndrome, including increased PG-34:1/PG-36:1 ratio and enrichment of very long polyunsaturated fatty acyl chains.[19] Our findings are further corroborated by the phenotypes of LPGAT1-deficient zebrafish, including developmental defects, poor survival rate, and increased unsaturation of phospholipid species.[44]

PG is subjected to remodeling of its fatty acyl chains after *de novo* synthesis in mitochondria to achieve mature acyl compositions, which takes place in the MAM where the majority of phospholipid remodeling enzymes are localized.[1,9] As a mitochondrial phospholipid, PG must be transported back to mitochondria. Since mitochondria are not connected to the vesicular transport system, phospholipid exchange between the two organelles is commonly believed to occur through organelle contacts, as exemplified by the ERMES (ER-mitochondria encounter structure) complex in yeast.[45] The ERMES complex tethers the two organelles and plays a pivotal role in mitochondrial phospholipid trafficking.[45] Consequently, deletion of ERMES leads to profound CL deficiency in yeast.[46] Several proteins, including PDZ domain containing 8 (PDZD8),[47] protein tyrosine phosphatase interacting protein 51 (PTPIP51),[48] and extended synaptotagmin 1 (E-Syt1),[49] have been identified to function as phospholipid transfer proteins at ER-mitochondria contact sites. Particularly, PDZD8 was identified as a structural and functional ortholog of the yeast ERMES protein Mmm1.[47] However, the molecular mechanisms underlying non-vesicular lipid transport across ER mitochondrial contact sites in mammalian cells remain largely unknown. In this study, we identified an unexpected role of LPGAT in mediating the transport of newly remodeled PG from ER to mitochondria through interaction with the PHB/TIM translocon. We show that LPGAT1 selectively interacted with multiple

components of the PHB/TIM translocon, including PHB1, PHB2, AFG3L2, TIMM23, TIMM50, TIMM44, and TIMM14. Using a *de novo* lipid labeling method recently developed by us,[27] we further demonstrated that interaction plays a pivotal role in coupling PG remodeling with mitochondrial trafficking of newly remodeled PG. Accordingly, we showed that ablation of TIMM14, a component of the PHB/TIM translocon, caused significant ER retention of newly remodeled PG, leading to aberrant acyl compositions of PG that were highly reminiscent of those caused by LPGAT1 deficiency. Consequently, ablation of TIMM14 also caused multiple defects in mitochondrial morphology and function similar to those caused by LPGAT1 deficiency, including near total loss of cristae structure, mtDNA depletion, oxidative stress, and defective oxidative phosphorylation. Our findings are corroborated by previous reports that mutations in the *TIMM14* gene in humans also led to MEGDEL-like syndrome, including mitochondrial dysfunction, dilated cardiomyopathy, deafness, and accumulation of 3-MGA in urine.[28,50]

Emerging evidence suggest that there is crosstalk between mitochondrial protein import and phospholipids.[51] In support of this notion, the PHB/TIM complexes, which are commonly recognized by their key role in mediating mitochondrial protein import, have also been shown to plays a key role in CL remodeling. Accordingly, ablation of the PHB/TIM complex caused defective CL remodeling.[30] Although the precise mechanisms by which PHB/TIM regulates CL remodeling remain poorly understood, the surprising finding that the PHB/TIM complex is required for mitochondrial PG trafficking provides a partial answer to this question, as PG is used for the synthesis of CL. Accordingly, TIMM14 deficiency also caused a profound alteration in the acyl chain compositions of CL, leading to significant enrichment of long-chain polyunsaturated fatty acids and deficiency in shorter and more saturated fatty acids. Remarkably, these defects were strikingly similar to aberrant PG species in cells deficient in LPGAT1, further implicating a pivotal role of the PHB/TIM complex in mitochondrial PG transport. However, whether the LPGAT1/PHB/TIM complex represents a mammalian ortholog of the yeast ERMES complex or a new ER mitochondrial encounter structure remains to be studied.

As part of the mitochondrial import motor, both PHBs and TIMs are primarily localized at the inner mitochondrial membrane. In contrast, our previous work showed that LPGAT1 was primarily localized at the MAM,[18] which raises an intriguing question about how LPGAT1 interacts with the PHB/TIM complex. We partly addressed this issue by identifying a pivotal role for MFN2 in mediating the interaction of LPGAT1 with the PHB/TIM complex. MFN2 is a mitochondrial GTPase that is required for tethering the ER with the outer mitochondrial membrane.[52] We found that MFN2 depletion not only attenuated the interaction of LPGAT1 with the PHB/TIM complex but also prevented the mitochondrial transport of newly remodeled PG from the ER, implicating an important role of MAM integrity in regulating the interaction of LPGAT1 with the PHB/TIM mitochondrial import motor. The findings are further corroborated by the results from STRING network analysis of the MFN2 interactome, which forms comprehensive interactions with multiple members of the PHB/TIM complex.

LPGAT1 was the first LPG acyltransferase previously identified by us.[1] Recently, two studies have demonstrated additional function of LPGAT1 in catalyzing the remodeling

of other phospholipids, including PE and PC.[53,54] These findings are in line with substrate promiscuity of most acyltransferases.[55] For example, acyl-CoA lysocardiolipin acyltransferase 1 (ALCAT1), which was first identified as a CL acyltransferase,[9] also recognizes both LPG and lysophosphatidylinositol as substrates.[56] Likewise, our previous work shows that monoacylglycerol acyltransferase 3 (MGAT3), which catalyzes the remodeling of triglycerides, also uses both monoacylglycerol and diacylglycerol as substrates.[57] Moreover, diacylglycerol acyltransferase-1 (DGAT1) catalyzes the remodeling of multiple structurally diversified lipids, including triglycerides, waxes, and retinyl esters.[58] Consistent with this notion, we also reported significant remodeling of both PC and PE in the liver of LPGAT1-deficient mice.[18] Although we could not rule out the involvement of both PE and PC in regulating the phenotype of LPGAT1 KO mice, multiple lines of evidence from the current study suggest that the major metabolic defects in the LPGAT1 KO mice were primarily caused by aberrant remodeling of PG and trafficking, as LPGAT1 deficiency selectively impaired mitochondrial PG transport from the ER but not other phospholipids, including CL, PE, and PC. Consequently, LPGAT1 deficiency also caused significant alteration of CL acyl compositions, leading to multiple defects in cristae structure, mtDNA biogenesis, and mitochondrial respiration.

Finally, a genetic linkage study has previously identified LPGAT1 as one of the three candidate genes at the genetic locus of *1q32.2-q32.3* for progressive familial heart block type II characterized by sudden cardiac death and dilated cardiomyopathy in humans.[22] However, there is very little information available about LPGAT1 mutations in humans to date. This is likely due to the fact that LPGAT1 mutations cause high fatality rate during development, as demonstrated by this study and the phenotype of LPGAT1-deficient zebrafish.[44] In addition to MEGDEL syndrome, an emerging group of rare human genetic diseases, including BTHS, Sengers syndrome, and DCMA, all share common clinical presentations, including dilated cardiomyopathy, skeletal muscle weakness, 3-MGA aciduria, and premature death,[39] yet the molecular mechanisms underlying these common defects remain poorly understood. Together, this study has not only provided experimental evidence for the human linkage analysis but has also identified a pivotal role of LPGAT1 in preventing mitochondrial dysfunction in MEGDEL syndrome, implicating a common mechanism underlying the causes of these rare genetic disorders through defective mitochondrial PG remodeling and transport.

Limitations of the study

A major shortfall of the current study is a lack of the precise mechanism by which the PHB/TIM complex regulates mitochondrial import of PG. In contrast to the ERMES complex in yeast, which comprises members with lipid-binding domains for glycerophospholipids, there is very little information on whether any members of the PHB/TIM complex possess lipid-binding activity. Another challenging issue originated from this study is whether LPGAT1 possesses lipid transfer activity, and if so, whether this putative activity is independent of its acyltransferase activity.

STAR★METHODS

RESOURCE AVAILABILITY

Lead contact—Further information and requests for resources and reagents should be directed to and will be fulfilled by the lead contact, Yuguang Shi (shiy4@uthscsa.edu).

Materials availability—All unique/stable reagents and mice generated in this study will be made available on request to the lead contact as indicated above, but we may require a completed materials transfer agreement if there is potential for commercial application.

Data and code availability

- All data reported in this paper will be shared by the lead contact by request.
- This paper does not report original code.
- Any additional information required to reanalyze the data reported in this paper is available from the lead contact upon request.

EXPERIMENTAL MODEL AND STUDY PARTICIPANT DETAILS

Mouse models—Mice with targeted deletion of the *LPGAT1* gene were generated as previously described.[18] 18 weeks old male *LPGAT1* knockout and age-matched *WT* control mice were used in all experiments unless specifically indicated. All animals were fed with normal diet (Teklad 5001 Laboratory Diet) and maintained in an environmentally controlled facility with diurnal light cycle and free access to water. The study protocols were approved by the Institutional Animal Care and Use Committee of Nanjing Medical University.

Cell culture—MEFs were prepared as previously described.[59] In brief, the female mice at embryonic day 12.5–13.5 were euthanized, and embryos were dissected out on a dish with HBSS. Head, limbs, and internal organs were removed. The remaining embryo was minced with a razor blade and transferred to a 15 mL tube with 4 mL of collagenase solution (2 mg/mL collagenase IV, 0.7 mg/mL DNase I and 10 mg/mL hyaluronidase). Tubes were rotated for 30–60 min in a 37°C incubator until all of the tissue chunks were gone. The digested solution was filtered through 100 μm mesh to 50 mL tubes filled with chilled DMEM (30 mL). The samples were centrifuged at 9,000 × g for 5 min, and the cell pellet was washed again with 25 mL of DMEM. Cells were then seeded with complete medium. Primary hepatocytes were isolated and cultured as previously described.[18,60]

MEFs, primary hepatocytes, C2C12, and HEK293T cells were cultured in DMEM medium supplemented with 10% fetal bovine serum, 100 U/mL penicillin and 100 mg/mL streptomycin at 37°C under 5% CO2. All cell lines tested negative for mycoplasma contamination.

METHOD DETAILS

Echocardiography—Echocardiographic analysis was performed using a Vevo 2100 Imaging System and an MS550D transducer (Visual Sonics, Toronto, ON, Canada). M-mode short axis and B-mode long axis images of the left ventricle were analyzed to measure the

following parameters, including interventricular septal end-diastole and end-systole (IVSd and IVSs, mm), left ventricular internal diameter end-diastole and end-systole (LVIDd and LVIDs, mm), left ventricular posterior wall end-diastole and end-systole (LVPWd and LVPWs, mm), left ventricular ejection fraction (LVEF), and left ventricular fractional shortening (LVFS) and heart rate (HR, bpm). Blood pressure and pulse were measured using BP-2000 (Visitech).

Auditory brainstem response (ABR) measurement—ABR measurements were performed by using the System 3 ABR workstation (Tucker Davis Technology) to assess mice auditory function. All tests were conducted in a soundproof room. Prior to the ABR measurement, animals were anesthetized by intraperitoneal injection of 100 mg/kg ketamine, and placed on a heating pad to maintain their body temperature at 37°C. A free-field magnetic speaker (model FF1, Tucker Davis Technology) was placed 10 cm from the left pinna. Computer-generated clicks (100 μs duration, with a spectrum of 0–50 kHz) and 5 ms pure tone stimuli of 4, 8, 12, 16, 24 and 32 kHz were presented with maximum intensities of 100 dB sound pressure level (SPL). Subdermal needle electrodes (S06666–0, Rochester Electro-Medical) were positioned at the apex of the skull (+ve), the left cheek (−ve) and the left hind leg (ground). The stimulus signals were generated using a SigGenRP and an RP2.1 real-time processor, and then transmitted through a programmable attenuator (PA5, TDT), a speaker driver (ED1, TDT), and an electrostatic speaker (EC1, TDT). Stimuli were generated for 1024 repetitions in 5–10 dB decrements, starting from a 90-dB sound pressure level to the acoustic threshold at every frequency. The phase of the stimulus was reversed upon each presentation to reduce the artifacts caused by repetitive stimuli.

Histological analysis—Mice were anesthetized with isoflurane, and the heart samples were carefully isolated and fixed in 4% paraformaldehyde for 48 h. Fixed hearts were dehydrated and embedded in paraffin, and 5 μm sections were cut with a Leica RM-2162 (Leica, Bensheim, Germany). H&E staining, Masson's trichrome staining, and Sirius red staining were performed as previously described.[18] Wheat germ agglutinin (WGA, 5 μg/ml, Thermo Fish Scientific) staining was performed in the heart sections by using Alexa Fluor 488 conjugate dye.

Serum and urine Biochemical analysis—Urine samples were collected from live animals by holding and lightly stroking the belly of the animals. The urine samples were collected in a clear plastic wrap, and transferred to 1.5 mL EP tubes. Serum samples were collected by centrifuge the whole blood for 15 min at 4°C. Biochemical analysis of the serum or urine samples was carried out using specific kits according to the manufacturer's instructions. 3-MGA in the urine was determined by gas chromatography-mass spectrometry.

Generation of gene knockout Cell lines by CRISPR/Cas9-mediated gene Editing—*LPGAT1*, *TIMM14*, or *MFN2* gene was knocked out in C2C12 cells by transfecting CRISPR/Cas9 mouse plasmids from Santa Cruz (#sc-432665 and #sc-432665-HDR for *LPGAT1*, #sc-426704 and #sc-426704-HDR for *TIMM14*, #sc-431291 and #sc-431291-HDR for *MFN2*) using Viafect transfection reagent (#E4982, Promega), and

then purified through GFP and RFP fluorescence by flow cytometry. Vector control cells were created by transfecting C2C12 cells with an empty pBABE-puro vector backbone (Addgene, #1764). All cells were then kept under selection with 5 μg/mL puromycin (#B7587, APExBIO). C2C12 cells were maintained at 37°C with 5% CO_2, cultured in high-glucose DMEM (#11965118, Gibco) supplemented with 10% FBS (#12483020, Gibco) and 50 mg/mL penicillin/streptomycin (#15140122, Invitrogen). Gene knockout was confirmed by Western blot using anti-LPGAT1, anti-TIMM14, or anti-MFN2 antibodies.

Quantitative real-time PCR analysis—The total RNA was extracted using the RNAiso Plus kit (#9108, Takara) according to the manufacturer's instructions. 1 μg of total RNA was reverse-transcribed to complementary DNA (cDNA) using the HiScript II Q RT SuperMix (#R222–01, Vazyme). cDNAs were then used as templates for quantification of genes expression by real-time PCR analysis, which was performed using the ChamQ SYBR qPCR Master Mix (#Q311–02, Vazyme) and the 7300 Real-Time PCR System (Applied Biosystems). GAPDH was used as the internal control. The primers used in PCR are shown in Table S1.

Transmission electron microscopy—The mitochondrial ultrastructure in cells was evaluated by using transmission electron microscopy. Cells were fixed in 5% glutaraldehyde and 4% paraformaldehyde in 0.1 M sodium cacodylate buffer (pH 7.4) with 0.05% $CaCl_2$ for 24 h. After washing in 0.1 M sodium cacodylate buffer, cells were fixed overnight in 0.1 M cacodylate buffer containing 1% OsO_4, dehydrated, and embedded in EMbed-812 resin. The sections were stained with 2% uranyl acetate, followed by 0.4% lead citrate, and viewed with a JEOL JEM-2200FS 200kV electron microscope (Electron Microscopy Sciences Core at the University of Texas Health Science Center at San Antonio).

Oxygen consumption rate (OCR) measurement—Cells were seeded in XF96 cell culture microplates, and the OCR was measured by real-time extracellular flux analyses with a Seahorse XF96 analyzer (Agilent, North Billerica, MA) in response to treatment with oligomycin (ATP synthase inhibitor, 1 μM), FCCP (oxidative phosphorylation uncoupler, 1 μM), and a mixture of rotenone (respiratory complex I inhibitor, 1 mM) and antimycin A (respiratory complex III inhibitor, 1 μM). Real-time OCR were averaged and recorded three times during each conditional cycle.

Live Cell fluorescence labeling and confocal imaging—For live cell confocal imaging analysis, cells were plated on 35 mm glass bottom imaging dishes. Cells were transfected with Mito-BFP or stained with MitoTracker-Red CMXRos (100 nM) to visualize mitochondria. The ER was visualized by transfecting cells with dsRed2-ER5. Nucleus was stained with Hoechst 33342 (10 μg/mL). *De novo* phospholipids labeling was followed as previously reported.[27] In brief, cells were first nutrient starved in a standard Krebs Ringer Phosphate HEPES buffer (KRPH, 140 mM NaCl, 2 mM Na_2HPO_4, 4 mM KCl, 1 mM $MgCl_2$, 1.5 mM $CaCl_2$, 10 mM HEPES, pH7.4) for 1 h, and then incubated with 16:0 NBD-acyl-CoA (1 μM) and 18:1 LPG (20 μM), 18:1 LPC (50 μM), 18:1 LPE (50 μM), or MLCL (50 μM) for indicated time. An Olympus FV1200 confocal microscope with a 63x oil inverted objective was used for live cell imaging.

Intracellular reactive oxygen species (ROS) analysis—Cells were seeded in 96 well assay plate at 8000 cells/well and cultured overnight. Intracellular ROS generation was measured using 2′,7′-dichlordehydrofluorescein-diacetate (DCFH-DA) at a final concentration of 10 mM in blank medium for 20 min at 37°C, then followed by washing 3 times with fresh empty medium. The fluorescence was measured using a SpectraMax M2 microplate reader (Molecular Devices) set to 488 nm excitation and 525 nm emission wavelengths.

Mitochondrial DNA (mtDNA) copy number assay—Genomic DNA was extracted using the multisource genomic DNA miniprep kit (AP-MN-MS-GDNA, Axygen) according to the manufacturer's instruction. mtDNA copy number was determined by PCR using mitochondrion-encoded NADH dehydrogenase 1 (ND1) as the mtDNA marker and cyclophilin A as the nuclear DNA marker. The primer for ND1 and cyclophilin A were shown in Table S1.

Cell transfection and immunoprecipitation assay—HEK293T cells were transfected with pcDNA3.1-FLAG-LPGAT1 or pcDNA3.1 vector plasmids using X-tremeGENE HP DNA transfection reagent according to the manufacturer's instructions. For knockdown of MFN2, cells were first transfected with control siRNA (SIC001, Sigma) or specific siRNA to MFN2 (SASI_Hs02_00330014, Sigma) using Lipofectamine RNAiMAX transfection reagent 6 h prior to plasmids transfection. After 30 h of transfection, cells were rinsed twice with ice-cold PBS and lysed in NP-40 lysis buffer (50 mM Tris-HCl, pH 7.5, 150 mM NaCl, 1 mM EDTA, 0.5% NP-40, 1 mM PMSF, and one tablet of EDTA-free protease inhibitors per 50mL). The soluble fractions from cell lysates were isolated by centrifugation at 12,000 rpm for 10 min at 4°C. Protein concentration was measured using Pierce BCA protein assay kit (Thermo Fisher, Cat#23225). For immunoprecipitations, primary anti-FLAG antibody was added to an equal amount of total protein from each lysate and incubated with rotation for 2 h at 4°C. 30 μL of a 50% slurry of protein A/G Sepharose beads was added and continuously incubated with rotation at 4°C overnight. The immunoprecipitants were then washed five times with lysis buffer, and 30 μL SDS sample buffer was added to the precipitates and boiled for 5 min to denature the proteins. The eluates were then resolved by 10% SDS-PAGE, and analyzed by Western blot analysis.

Lipids extraction and TLC analysis—To determine the newly remodeled PG, cells were incubated with 16:0 NBD-acyl-CoA (1 μM) and 18:1 LPG (20 μM) for 15 min. Mitochondria was isolated and purified according to the method described previously.[61] Total lipids from whole cells or isolated mitochondria were extracted using chloroform/methanol (2:1, v/v). The lipid samples were loaded to a TLC plate (Sigma, #60805), and developed in chloroform: methanol: water (65:25:4, v/v/v). The *in vitro* NBD labeled PG (NBD-PG) was used as a marker. The TLC plates were dried after development and scanned using a Typhoon 9410 Scanner.

Lipidomic analysis—The lipidomic analysis was carried out using methods previously described.[6,18] Briefly, total lipids from cells were analyzed by triple-quadruple mass spectrometer (Thermo Electron TSQ Quantum Ultra, Trzin, Slovenia) controlled by

Xcalibur (Thermo Fisher Scientific) system software. All the mass spectrometer spectra and tandem mass spectrometer spectra were acquired automatically by a customized sequence subroutine operated under Xcalibur software.

QUANTIFICATION AND STATISTICAL ANALYSIS

Statistical analysis—Mice survival rate was conducted by Kaplan-Meyer survival analysis, and statistical difference was done by Log rank (Mantel-Cox) test. Data are routinely represented as means ± SD. Statistical significance was assessed by two-tailed non-paired t-tests using GraphPad Prism 7.0. Differences were considered statistically significant at $p < 0.05$; *$p < 0.05$; **$p < 0.01$; ***$p < 0.001$.

Supplementary Material

Refer to Web version on PubMed Central for supplementary material.

ACKNOWLEDGMENTS

We would like to thank Dr. Jia Nie for techincal support in mitochondrial phospholipid trafficking analysis. The current studies were funded in part by the National Institutes of Health, United States (R01AG055747, R01DK133463, R01AG081422, and P30AG013319, Y.S.), the American Diabetes Association, United States (#1–18-IBS-329, Y.S.), the Barth Syndrome Foundation, United States (J.Z.), the Nathan Shock Center Pilot Grants Program (J.Z.), and an endowment from the Joe R. and Teresa Lozano Long Distinguished Chair in Metabolic Biology (Y.S.).

INCLUSION AND DIVERSITY

We worked to ensure sex balance in the selection of non-human subjects. We worked to ensure diversity in experimental samples through the selection of the cell lines.

REFERENCES

1. Yang Y, Cao J, and Shi Y (2004). Identification and characterization of a gene encoding human LPGAT1, an endoplasmic reticulum-associated lysophosphatidylglycerol acyltransferase. J. Biol. Chem. 279, 55866–55874. 10.1074/jbc.M406710200. [PubMed: 15485873]
2. Chang SC, Heacock PN, Clancey CJ, and Dowhan W (1998). The PEL1 gene (renamed PGS1) encodes the phosphatidylglycero-phosphate synthase of Saccharomyces cerevisiae. J. Biol. Chem. 273, 9829–9836. 10.1074/jbc.273.16.9829. [PubMed: 9545322]
3. Chen D, Zhang XY, and Shi Y (2006). Identification and functional characterization of hCLS1, a human cardiolipin synthase localized in mitochondria. Biochem. J. 398, 169–176. 10.1042/BJ20060303. [PubMed: 16716149]
4. Zhang J, Guan Z, Murphy AN, Wiley SE, Perkins GA, Worby CA, Engel JL, Heacock P, Nguyen OK, Wang JH, et al. (2011). Mitochondrial phosphatase PTPMT1 is essential for cardiolipin biosynthesis. Cell Metabol. 13, 690–700. 10.1016/j.cmet.2011.04.007.
5. Tamura Y, Harada Y, Nishikawa S.i., Yamano K, Kamiya M, Shiota T, Kuroda T, Kuge O, Sesaki H, Imai K, et al. (2013). Tam41 is a CDP-diacylglycerol synthase required for cardiolipin biosynthesis in mitochondria. Cell Metabol. 17, 709–718. 10.1016/j.cmet.2013.03.018.
6. Li J, Romestaing C, Han X, Li Y, Hao X, Wu Y, Sun C, Liu X, Jefferson LS, Xiong J, et al. (2010). Cardiolipin remodeling by ALCAT1 links oxidative stress and mitochondrial dysfunction to obesity. Cell Metabol. 12, 154–165. 10.1016/j.cmet.2010.07.003.
7. Zhang J, Liu X, Nie J, and Shi Y (2022). Restoration of mitophagy ameliorates cardiomyopathy in Barth syndrome. Autophagy 18, 2134–2149. 10.1080/15548627.2021.2020979. [PubMed: 34985382]

8. Hsu P, Liu X, Zhang J, Wang HG, Ye JM, and Shi Y (2015). Cardiolipin remodeling by TAZ/tafazzin is selectively required for the initiation of mitophagy. Autophagy 11, 643–652. 10.1080/15548627.2015.1023984. [PubMed: 25919711]
9. Cao J, Liu Y, Lockwood J, Burn P, and Shi Y (2004). A novel cardiolipin-remodeling pathway revealed by a gene encoding an endoplasmic reticulum-associated acyl-CoA:lysocardiolipin acyltransferase (ALCAT1) in mouse. J. Biol. Chem. 279, 31727–31734. 10.1074/jbc.M402930200. [PubMed: 15152008]
10. Hallman M, and Gluck L (1975). Phosphatidylglycerol in lung surfactant. II. Subcellular distribution and mechanism of biosynthesis in vitro. Biochim. Biophys. Acta 409, 172–191. 10.1016/0005-2760(75)90152-6. [PubMed: 172134]
11. Hallman M, Kulovich M, Kirkpatrick E, Sugarman RG, and Gluck L (1976). Phosphatidylinositol and phosphatidylglycerol in amniotic fluid: indices of lung maturity. Am. J. Obstet. Gynecol. 125, 613–617. 10.1016/0002-9378(76)90782-1. [PubMed: 180804]
12. Jiang F, Ryan MT, Schlame M, Zhao M, Gu Z, Klingenberg M, Pfanner N, and Greenberg ML (2000). Absence of cardiolipin in the crd1 null mutant results in decreased mitochondrial membrane potential and reduced mitochondrial function. J. Biol. Chem. 275, 22387–22394. [PubMed: 10777514]
13. Pokorná L, Čermáková P, Horváth A, Baile MG, Claypool SM, Griač P, Malínský J, and Balážová M (2016). Specific degradation of phosphatidylglycerol is necessary for proper mitochondrial morphology and function. Biochim. Biophys. Acta 1857, 34–45. 10.1016/j.bbabio.2015.10.004. [PubMed: 26482708]
14. Claypool SM, and Koehler CM (2012). The complexity of cardiolipin in health and disease. Trends Biochem. Sci. 37, 32–41. 10.1016/j.tibs.2011.09.003. [PubMed: 22014644]
15. Shi Y (2010). Emerging roles of cardiolipin remodeling in mitochondrial dysfunction associated with diabetes, obesity, and cardiovascular diseases. J. Biomed. Res. 24, 6–15. [PubMed: 23554606]
16. Hsu P, and Shi Y (2017). Regulation of autophagy by mitochondrial phospholipids in health and diseases. Biochim. Biophys. Acta Mol. Cell Biol. Lipids 1862, 114–129. 10.1016/j.bbalip.2016.08.003.
17. Gorden DL, Ivanova PT, Myers DS, McIntyre JO, VanSaun MN, Wright JK, Matrisian LM, and Brown HA (2011). Increased diacylglycerols characterize hepatic lipid changes in progression of human nonalcoholic fatty liver disease; comparison to a murine model. PLoS One 6, e22775. 10.1371/journal.pone.0022775. [PubMed: 21857953]
18. Zhang X, Zhang J, Sun H, Liu X, Zheng Y, Xu D, Wang J, Jia D, Han X, Liu F, et al. (2019). Defective Phosphatidylglycerol Remodeling Causes Hepatopathy, Linking Mitochondrial Dysfunction to Hepatosteatosis. Cell. Mol. Gastroenterol. Hepatol. 7, 763–781. 10.1016/j.jcmgh.2019.02.002. [PubMed: 30831319]
19. Wortmann SB, Vaz FM, Gardeitchik T, Vissers LELM, Renkema GH, Schuurs-Hoeijmakers JHM, Kulik W, Lammens M, Christin C, Kluijtmans LAJ, et al. (2012). Mutations in the phospholipid remodeling gene SERAC1 impair mitochondrial function and intracellular cholesterol trafficking and cause dystonia and deafness. Nat. Genet. 44, 797–802. 10.1038/ng.2325. [PubMed: 22683713]
20. Finsterer J, Scorza FA, Fiorini AC, and Scorza CA (2020). MEGDEL Syndrome. Pediatr. Neurol. 110, 25–29. 10.1016/j.pediatrneurol.2020.03.009. [PubMed: 32684373]
21. Sarig O, Goldsher D, Nousbeck J, Fuchs-Telem D, Cohen-Katsenelson K, Iancu TC, Manov I, Saada A, Sprecher E, and Mandel H (2013). Infantile mitochondrial hepatopathy is a cardinal feature of MEGDEL syndrome (3-methylglutaconic aciduria type IV with sensorineural deafness, encephalopathy and Leigh-like syndrome) caused by novel mutations in SERAC1. Am. J. Med. Genet. 161A, 2204–2215. 10.1002/ajmg.a.36059. [PubMed: 23918762]
22. Fernandez P, Moolman-Smook J, Brink P, and Corfield V (2005). A gene locus for progressive familial heart block type II (PFHBII) maps to chromosome 1q32.2-q32.3. Hum. Genet. 118, 133–137. 10.1007/s00439-005-0029-5. [PubMed: 16086176]
23. Barth PG, Valianpour F, Bowen VM, Lam J, Duran M, Vaz FM, and Wanders RJA (2004). X-linked cardioskeletal myopathy and neutropenia (Barth syndrome): an update. Am. J. Med. Genet. 126A, 349–354. [PubMed: 15098233]

24. Schlame M, and Ren M (2006). Barth syndrome, a human disorder of cardiolipin metabolism. FEBS Lett. 580, 5450–5455. [PubMed: 16973164]
25. Zhang J, and Shi Y (2022). In Search of the Holy Grail: Toward a Unified Hypothesis on Mitochondrial Dysfunction in Age-Related Diseases. Cells 11. 10.3390/cells11121906.
26. Mokranjac D, Sichting M, Neupert W, and Hell K (2003). Tim14, a novel key component of the import motor of the TIM23 protein translocase of mitochondria. EMBO J. 22, 4945–4956. 10.1093/emboj/cdg485. [PubMed: 14517234]
27. Zhang J, Nie J, Sun H, Li J, Andersen JP, and Shi Y (2022). De novo labeling and trafficking of individual lipid species in live cells. Mol. Metabol. 61, 101511. 10.1016/j.molmet.2022.101511.
28. Davey KM, Parboosingh JS, McLeod DR, Chan A, Casey R, Ferreira P, Snyder FF, Bridge PJ, and Bernier FP (2006). Mutation of DNAJC19, a human homologue of yeast inner mitochondrial membrane co-chaperones, causes DCMA syndrome, a novel autosomal recessive Barth syndrome-like condition. J. Med. Genet. 43, 385–393. 10.1136/jmg.2005.036657. [PubMed: 16055927]
29. Dweikat IM, Abdelrazeq S, Ayesh S, and Jundi T (2015). MEGDEL Syndrome in a Child From Palestine: Report of a Novel Mutation in SERAC1 Gene. J. Child Neurol. 30, 1053–1056. 10.1177/0883073814541474. [PubMed: 25051967]
30. Richter-Dennerlein R, Korwitz A, Haag M, Tatsuta T, Dargazanli S, Baker M, Decker T, Lamkemeyer T, Rugarli EI, and Langer T (2014). DNAJC19, a mitochondrial cochaperone associated with cardiomyopathy, forms a complex with prohibitins to regulate cardiolipin remodeling. Cell Metabol. 20, 158–171. 10.1016/j.cmet.2014.04.016.
31. Wortmann S, Rodenburg RJT, Huizing M, Loupatty FJ, de Koning T, Kluijtmans LAJ, Engelke U, Wevers R, Smeitink JAM, and Morava E (2006). Association of 3-methylglutaconic aciduria with sensorineural deafness, encephalopathy, and Leigh-like syndrome (MEGDEL association) in four patients with a disorder of the oxidative phosphorylation. Mol. Genet. Metabol. 88, 47–52. 10.1016/j.ymgme.2006.01.013.
32. Skoe E, and Kraus N (2010). Auditory brain stem response to complex sounds: a tutorial. Ear Hear. 31, 302–324. 10.1097/AUD.0b013e3181cdb272. [PubMed: 20084007]
33. Ikon N, and Ryan RO (2017). Cardiolipin and mitochondrial cristae organization. Biochim. Biophys. Acta Biomembr. 1859, 1156–1163. 10.1016/j.bbamem.2017.03.013. [PubMed: 28336315]
34. Hu C, Shu L, Huang X, Yu J, Li l., Gong L, Yang M, Wu Z, Gao Z, Zhao Y, et al. (2020). OPA1 and MICOS Regulate mitochondrial crista dynamics and formation. Cell Death Dis. 11, 940. 10.1038/s41419-020-03152-y. [PubMed: 33130824]
35. Glancy B, Kim Y, Katti P, and Willingham TB (2020). The Functional Impact of Mitochondrial Structure Across Subcellular Scales. Front. Physiol. 11, 541040. 10.3389/fphys.2020.541040. [PubMed: 33262702]
36. Flis VV, and Daum G (2013). Lipid transport between the endoplasmic reticulum and mitochondria. Cold Spring Harbor Perspect. Biol. 5, a013235. 10.1101/cshperspect.a013235.
37. Osman C, Voelker DR, and Langer T (2011). Making heads or tails of phospholipids in mitochondria. J. Cell Biol. 192, 7–16. 10.1083/jcb.201006159. [PubMed: 21220505]
38. Osman C, Haag M, Potting C, Rodenfels J, Dip PV, Wieland FT, Brügger B, Westermann B, and Langer T (2009). The genetic interactome of prohibitins: coordinated control of cardiolipin and phosphatidylethanolamine by conserved regulators in mitochondria. J. Cell Biol. 184, 583–596. 10.1083/jcb.200810189. [PubMed: 19221197]
39. Lamari F, Mochel F, Sedel F, and Saudubray JM (2013). Disorders of phospholipids, sphingolipids and fatty acids biosynthesis: toward a new category of inherited metabolic diseases. J. Inherit. Metab. Dis. 36, 411–425. 10.1007/s10545-012-9509-7. [PubMed: 22814679]
40. Ran Q, Wadhwa R, Kawai R, Kaul SC, Sifers RN, Bick RJ, Smith JR, and Pereira-Smith OM (2000). Extramitochondrial localization of mortalin/mthsp70/PBP74/GRP75. Biochem. Biophys. Res. Commun. 275, 174–179. 10.1006/bbrc.2000.3237. [PubMed: 10944461]
41. Christie DA, Lemke CD, Elias IM, Chau LA, Kirchhof MG, Li B, Ball EH, Dunn SD, Hatch GM, and Madrenas J (2011). Stomatin-like protein 2 binds cardiolipin and regulates mitochondrial biogenesis and function. Mol. Cell Biol. 31, 3845–3856. 10.1128/MCB.05393-11. [PubMed: 21746876]

42. Sassano ML, Felipe-Abrio B, and Agostinis P (2022). ER-mitochondria contact sites; a multifaceted factory for Ca(2+) signaling and lipid transport. Front. Cell Dev. Biol. 10, 988014. 10.3389/fcell.2022.988014. [PubMed: 36158205]
43. de Brito OM, and Scorrano L (2008). Mitofusin 2 tethers endoplasmic reticulum to mitochondria. Nature 456, 605–610. 10.1038/nature07534. [PubMed: 19052620]
44. Shibata T, Kawana H, Nishino Y, Ito Y, Sato H, Onishi H, Kano K, Inoue A, Taketomi Y, Murakami M, et al. (2022). Abnormal male reproduction and embryonic development induced by downregulation of a phospholipid fatty acid-introducing enzyme Lpgat1 in zebrafish. Sci. Rep. 12, 7312. 10.1038/s41598-022-11002-4. [PubMed: 35508627]
45. Kornmann B, Currie E, Collins SR, Schuldiner M, Nunnari J, Weissman JS, and Walter P (2009). An ER-mitochondria tethering complex revealed by a synthetic biology screen. Science 325, 477–481. 10.1126/science.1175088. [PubMed: 19556461]
46. Tamura Y, Onguka O, Hobbs AEA, Jensen RE, Iijima M, Claypool SM, and Sesaki H (2012). Role for two conserved intermembrane space proteins, Ups1p and Ups2p, [corrected] in intra-mitochondrial phospholipid trafficking. J. Biol. Chem. 287, 15205–15218. 10.1074/jbc.M111.338665. [PubMed: 22403410]
47. Hirabayashi Y, Kwon SK, Paek H, Pernice WM, Paul MA, Lee J, Erfani P, Raczkowski A, Petrey DS, Pon LA, and Polleux F (2017). ER-mitochondria tethering by PDZD8 regulates Ca(2+) dynamics in mammalian neurons. Science 358, 623–630. 10.1126/science.aan6009. [PubMed: 29097544]
48. Yeo HK, Park TH, Kim HY, Jang H, Lee J, Hwang GS, Ryu SE, Park SH, Song HK, Ban HS, et al. (2021). Phospholipid transfer function of PTPIP51 at mitochondria-associated ER membranes. EMBO Rep. 22, e51323. 10.15252/embr.202051323. [PubMed: 33938112]
49. Sassano ML, van Vliet AR, Vervoort E, Van Eygen S, Van den Haute C, Pavie B, Roels J, Swinnen JV, Spinazzi M, Moens L, et al. (2023). PERK recruits E-Syt1 at ER-mitochondria contacts for mitochondrial lipid transport and respiration. J. Cell Biol. 222, e202206008. 10.1083/jcb.202206008. [PubMed: 36821088]
50. Ucar SK, Mayr JA, Feichtinger RG, Canda E, Çoker M, and Wortmann SB (2017). Previously Unreported Biallelic Mutation in DNAJC19: Are Sensorineural Hearing Loss and Basal Ganglia Lesions Additional Features of Dilated Cardiomyopathy and Ataxia (DCMA) Syndrome? JIMD Rep. 35, 39–45. 10.1007/8904_2016_23. [PubMed: 27928778]
51. Hoffmann JJ, and Becker T (2022). Crosstalk between Mitochondrial Protein Import and Lipids. Int. J. Mol. Sci. 23, 5274. 10.3390/ijms23095274. [PubMed: 35563660]
52. Merkwirth C, and Langer T (2008). Mitofusin 2 builds a bridge between ER and mitochondria. Cell 135, 1165–1167. 10.1016/j.cell.2008.12.005. [PubMed: 19109886]
53. Kawana H, Ozawa M, Shibata T, Onishi H, Sato Y, Kano K, Shindou H, Shimizu T, Kono N, and Aoki J (2022). Identification and characterization of LPLAT7 as an sn-1-specific lysophospholipid acyltransferase. J. Lipid Res. 63, 100271. 10.1016/j.jlr.2022.100271. [PubMed: 36049524]
54. Xu Y, Miller PC, Phoon CKL, Ren M, Nargis T, Rajan S, Hussain MM, and Schlame M (2022). LPGAT1 controls the stearate/palmitate ratio of phosphatidylethanolamine and phosphatidylcholine in sn-1 specific remodeling. J. Biol. Chem. 298, 101685. 10.1016/j.jbc.2022.101685. [PubMed: 35131264]
55. Hishikawa D, Shindou H, Kobayashi S, Nakanishi H, Taguchi R, and Shimizu T (2008). Discovery of a lysophospholipid acyltransferase family essential for membrane asymmetry and diversity. Proc. Natl. Acad. Sci. USA 105, 2830–2835. 10.1073/pnas.0712245105. [PubMed: 18287005]
56. Zhao Y, Chen YQ, Li S, Konrad RJ, and Cao G (2009). The microsomal cardiolipin remodeling enzyme acyl-CoA lysocardiolipin acyltransferase is an acyltransferase of multiple anionic lysophospholipids. J. Lipid Res. 50, 945–956. 10.1194/jlr.M800567-JLR200. [PubMed: 19075029]
57. Cao J, Cheng L, and Shi Y (2007). Catalytic properties of MGAT3, a putative triacylglycerol synthase. J. Lipid Res. 48, 583–591. [PubMed: 17170429]
58. Yen CLE, Monetti M, Burri BJ, and Farese RV Jr. (2005). The triacylglycerol synthesis enzyme DGAT1 also catalyzes the synthesis of diacylglycerols, waxes, and retinyl esters. J. Lipid Res. 46, 1502–1511. 10.1194/jlr.M500036-JLR200. [PubMed: 15834126]

59. Li J, Liu X, Wang H, Zhang W, Chan DC, and Shi Y (2012). Lysocardiolipin acyltransferase 1 (ALCAT1) controls mitochondrial DNA fidelity and biogenesis through modulation of MFN2 expression. Proc. Natl. Acad. Sci. USA 109, 6975–6980. 10.1073/pnas.1120043109. [PubMed: 22509026]

60. Wang L, Liu X, Nie J, Zhang J, Kimball SR, Zhang H, Zhang WJ, Jefferson LS, Cheng Z, Ji Q, and Shi Y (2015). ALCAT1 controls mitochondrial etiology of fatty liver diseases, linking defective mitophagy to steatosis. Hepatology 61, 486–496. 10.1002/hep.27420. [PubMed: 25203315]

61. Wieckowski MR, Giorgi C, Lebiedzinska M, Duszynski J, and Pinton P (2009). Isolation of mitochondria-associated membranes and mitochondria from animal tissues and cells. Nat. Protoc. 4, 1582–1590. 10.1038/nprot.2009.151 [PubMed: 19816421]

Highlights

- LPGAT1 specifically interacts with PHB/TIM translocon
- LPGAT1 coordinates with PHB/TIM translocon for mitochondrial PG transport
- Loss of LPGAT1 or TIMM14 causes similar aberrant PG acyl compositions
- Ablation of LPGAT1 causes cardinal features of MEGDEL syndrome in mice

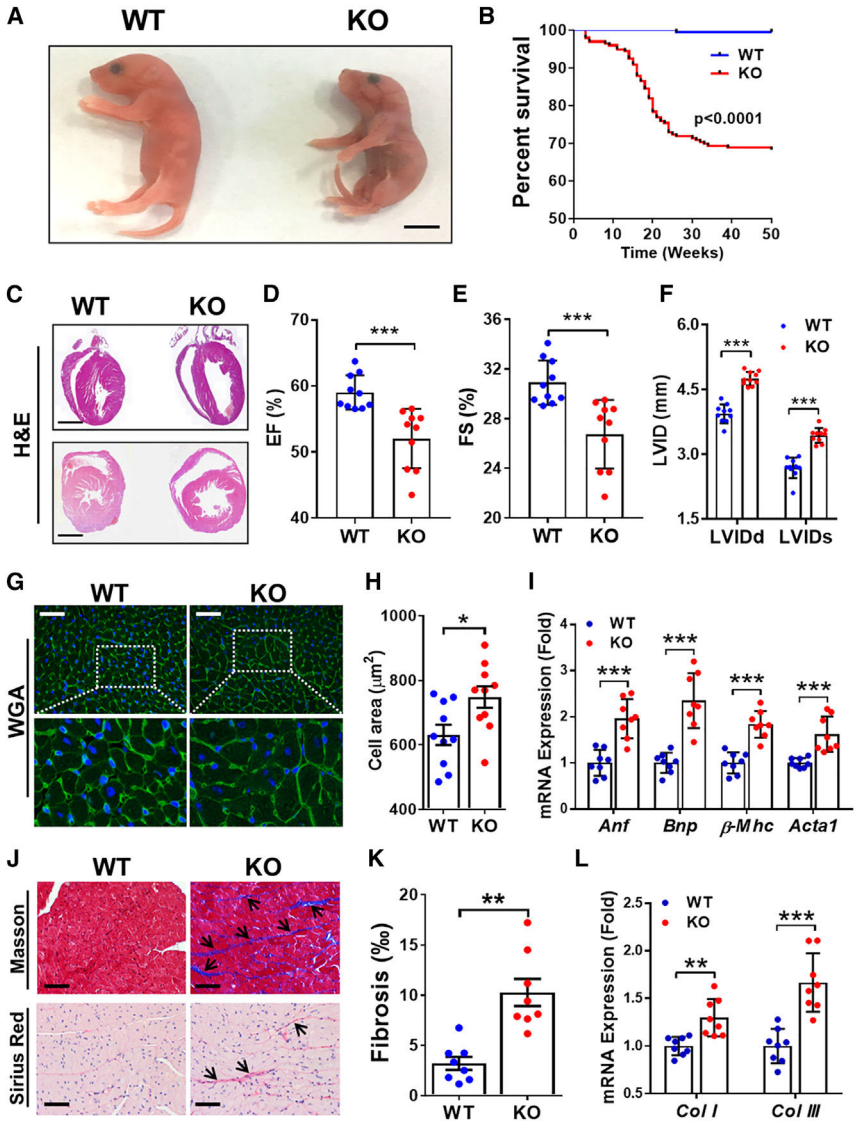

Figure 1. Ablation of LPGAT1 causes dilated cardiomyopathy and premature death in mice

(A) Representative images of neonatal WT control and LPGAT1 KO mice. Scale bar, 5 mm.

(B) Kaplan-Meyer survival analysis of WT control and LPGAT1 KO mice. n = 209–212. Statistical difference was done by log-rank (Mantel-Cox) test.

(C) Representative images of hematoxylin and eosin (H&E) staining of transverse and longitudinal sections of 18-week-old WT control and LPGAT1 KO mice hearts. Scale bar, 2 mm.

(D–F) Echocardiographic analysis of LV ejection fraction (EF; D), LV fractional shortening (FS; E), and LV internal diameter at end systole and at end diastole (LVIDs and LVIDd, respectively; F) of 18-week-old WT control and LPGAT1 KO mice. n = 10.

(G) Representative images of wheat germ agglutinin (WGA) staining of left ventricle sections. Scale bar, 100 μm.

(H) Quantification analysis of the cardiomyocytes size in left ventricle, related to (G). n = 10.

(I) Quantitative real-time PCR analysis of the mRNA levels of key biomarkers associated with cardiac hypertrophy, including atrial natriuretic factor (*Anf*), brain natriuretic peptide (*Bnp*), β-myosin heavy chain (*β-Mhc*), and skeletal muscle α-actin (*Aata1*). n = 8.
(J) Representative images of Masson's trichrome and Sirius red staining of fibrosis (highlight by arrows) of the heart sections. Scale bar, 100 μm.
(K) Quantification of the area of fibrosis in the heart, related to (J). n = 8.
(L) Quantitative real-time PCR analysis of the mRNA levels of collagen-I (*Col I*) and *Col III* in mice heart. n = 8.
Data are expressed as mean ± SD; *p < 0.05, **p < 0.01, and ***p < 0.001 by Student's t test.

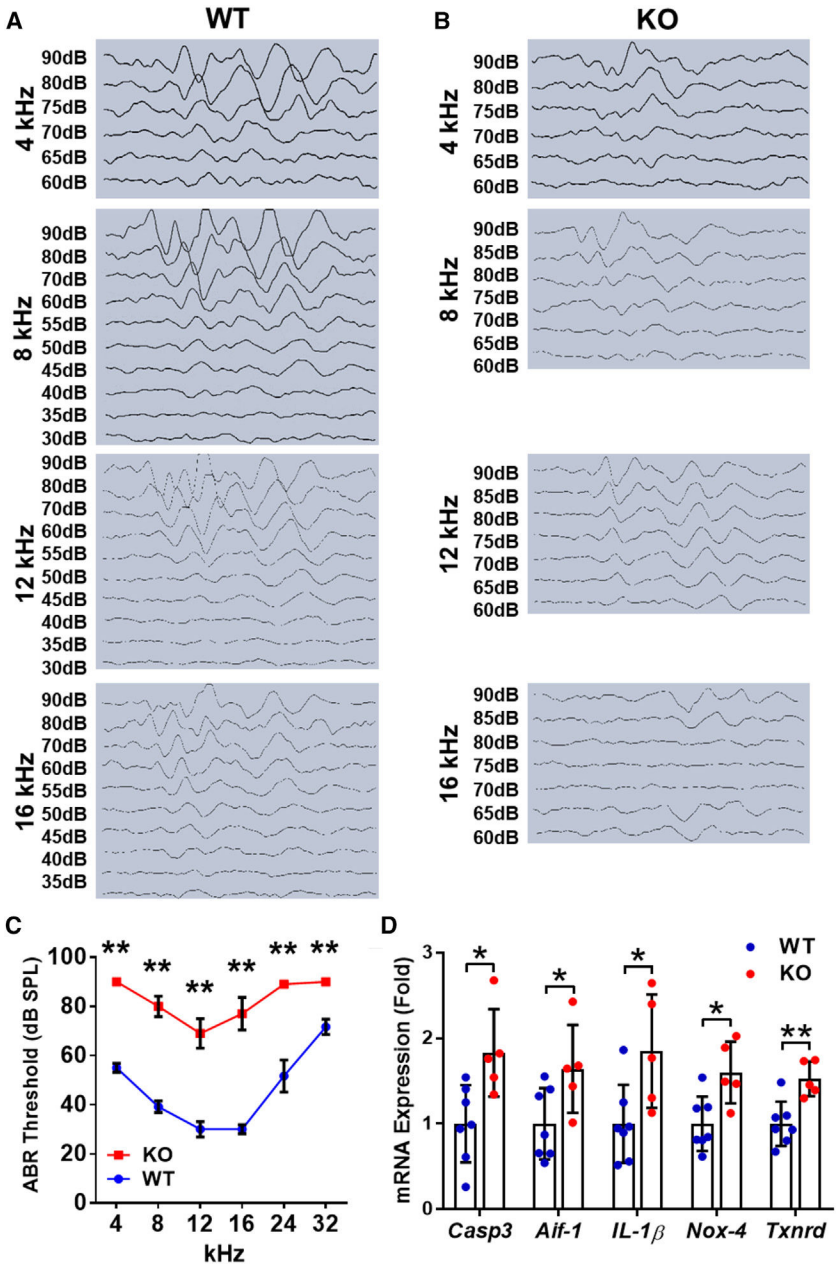

Figure 2. LPGAT1 deficiency induces hearing loss in mice

(A and B) Representative auditory brainstem response (ABR) waveform recordings in response to 4–16 kHz tone-pip stimuli from WT control (A) and LPGAT1 KO (B) mice. ABR click stimuli were provided from 90 to 10 dB sound pressure level (SPL) in 5–10 dB descending intervals.

(C) Quantification analysis of ABR thresholds to click and tone-pip stimuli (4–32 kHz). n = 5–6.

(D) Quantitative real-time PCR analysis of the mRNA levels of caspase-3 (*Casp3*), allograft inflammatory factor 1 (*Aif-1*), interleukin-1β (*IL-1β*), NADPH oxidase 4 (*Nox-4*), and thioredoxin reductase (*Txnrd*) in cochlear. n = 5–7.

Data are expressed as mean ± SD; *p < 0.05 and **p < 0.01 by Student's t test.

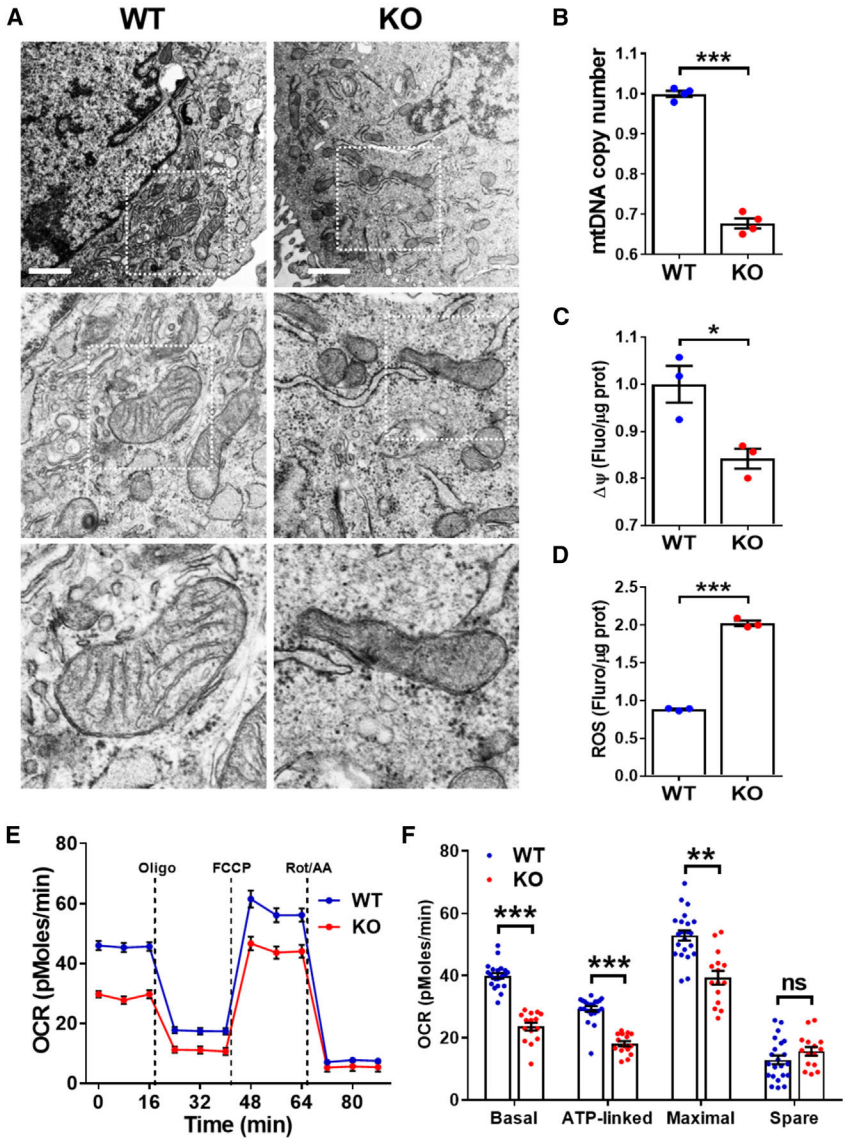

Figure 3. Ablation of LPGAT1 leads to defective cristae structure and mitochondrial dysfunction

(A) EM analysis of mitochondrial morphology in MEFs isolated from WT control and LPGAT1 KO mice. Scale bar, 1 μm.

(B) PCR analysis of mtDNA copy number of WT and LPGAT1 KO MEFs. n = 4.

(C) Analysis of the mitochondrial membrane potential of WT and LPGAT1 KO MEFs. n = 3.

(D) Analysis of intracellular ROS level in WT and LPGAT1 KO MEFs. n = 3.

(E–F) Seahorse XF analysis (E) and quantification of OCR (F) of WT control and LPGAT1 KO MEFs.

Data are expressed as mean ± SD; **p < 0.01 and ***p < 0.001. ns, non-significant, by Student's t test.

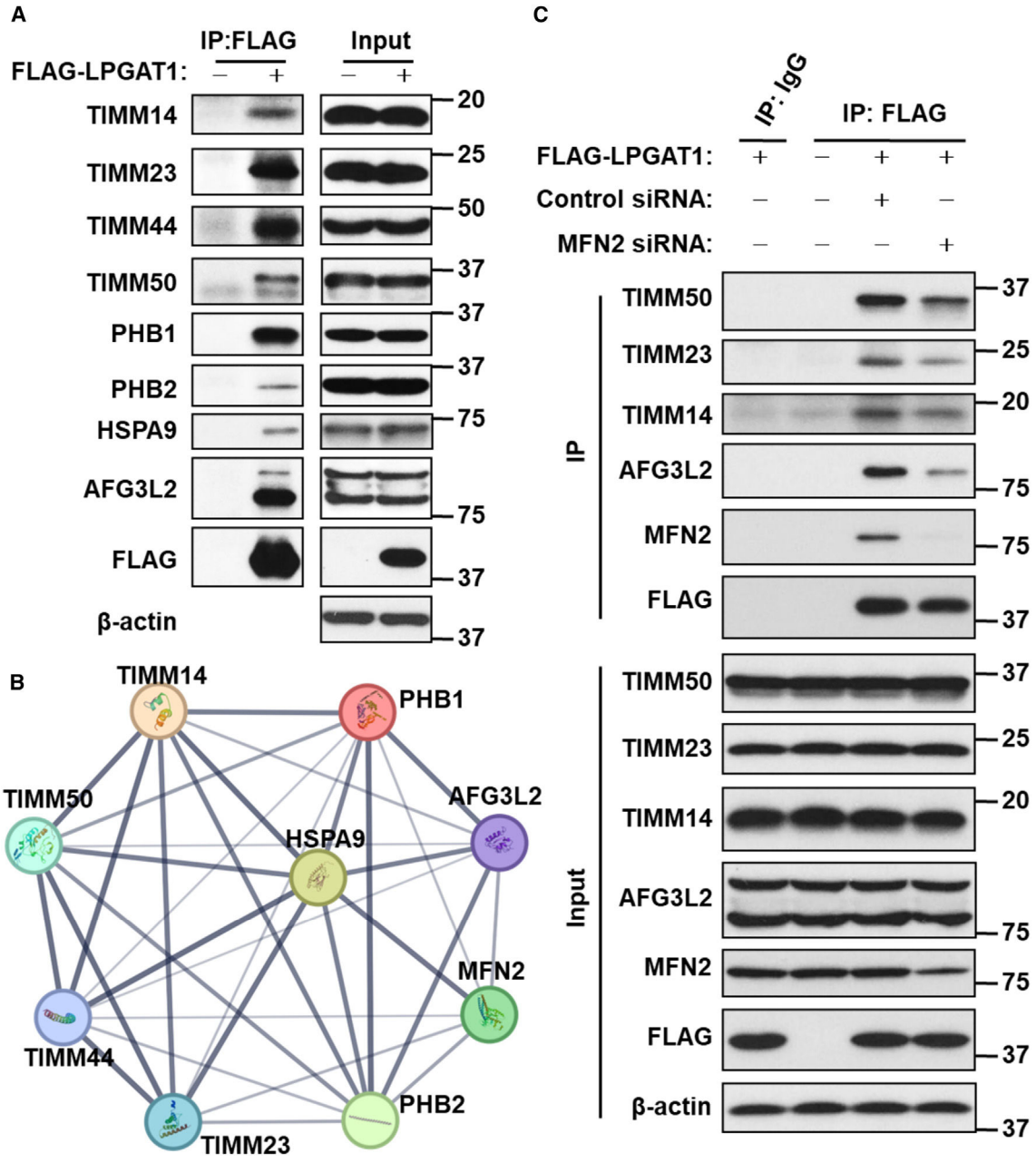

Figure 4. LPGAT1 interacts with the PHB/TIM complex

(A) coIP analysis of the interaction of LPGAT1 with indicated proteins of PHB/TIM complex in HEK293T cells transiently expressing FLAG-LPGAT1.

(B) STRING analysis of the protein interaction network of PHB/TIM complex with MFN2. The thickness of the lines indicates the confidence of interaction between two proteins.

(C) coIP analysis of the interaction of LPGAT1 with the indicated members of PHB/TIM complex in HEK293T cells transiently expressing FLAG-LPGAT1 and specifically knockdown of MFN2 by siRNA.

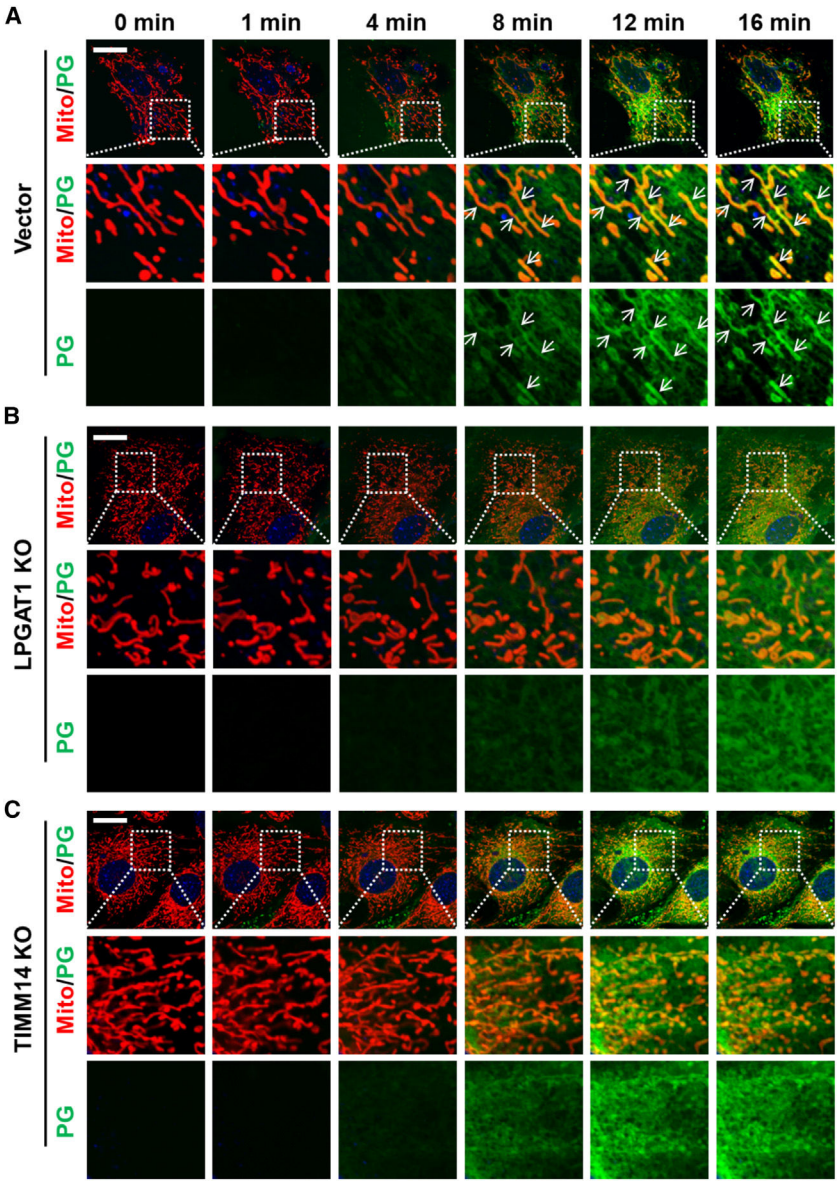

Figure 5. LPGAT1 and TIMM14 are required for mitochondrial PG transport

(A–C) Time-lapse confocal imaging analysis of NBD labeling and mitochondrial transport of PG in C2C12 vector control (A), LPGAT1 KO (B), and TIMM14 KO (C) cells. Cells were starved in Krebs Ringer Phosphate HEPES buffer (KRPH) for 1 h, followed by incubation with 18:1 LPG (20 μM) and 16:0 NBD-acyl-CoA (1 μM) for the indicated times. Mitochondria were stained with MitoTracker Red. Arrows highlight the co-localization of NBD-PG with mitochondria. Scale bar: 20 μm.

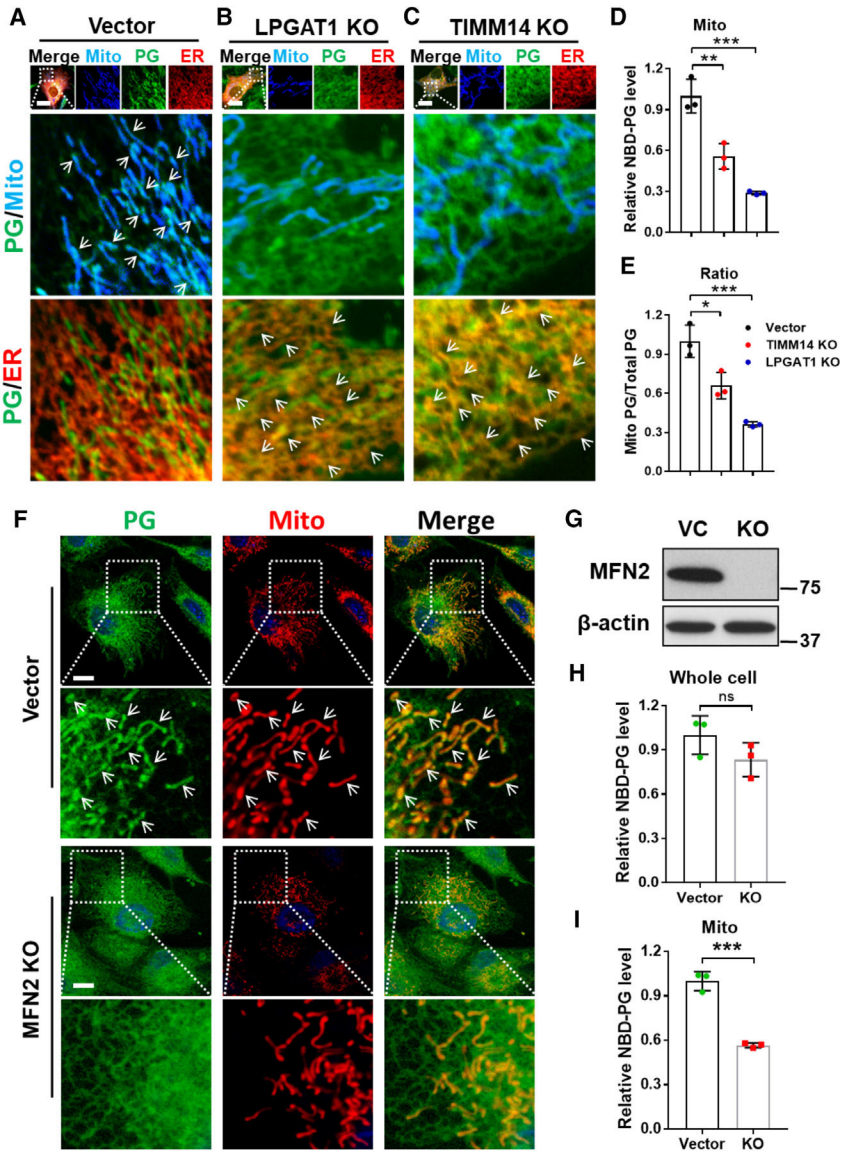

Figure 6. LPGAT1- and TIMM14-mediated mitochondrial PG transport requires integrity of the MAM

(A–C) Confocal imaging analysis of mitochondrial PG transport in live C2C12 vector control (A), LPGAT1 KO (B), and TIMM14 KO cells (C). Cells were transfected with Mito-BFP and dsRed2-ER5 to label mitochondria and the ER, respectively, and then starved in KRPH for 1 h, followed by incubation with 18:1 LPG (20 μM) and 16:0 NBD-acyl-CoA (1 μM) for 15 min. Arrows in PG/Mito or PG/ER panels highlight the co-localization of NBD-PG with mitochondria or the ER, respectively. Scale bar, 20 μm.

(D and E) Quantitative analysis of relative NBD-PG levels in isolated mitochondria (D) and the ratio of mitochondrial NBD-PG to total NBD-PG (E) in vector control, LPGAT1 KO, and TIMM14 KO cells.

(F) Confocal imaging analysis of NBD labeling and mitochondrial transport of PG in C2C12 vector control and MFN2 KO cells. Arrows in enlarged panel of vector control cells highlight the co-localization of NBD-PG with mitochondria. Scale bar, 10 μm.

(G) Western blot analysis of MFN2 protein expression in C2C12 vector control and MFN2 KO cells.

(H and I) Quantitative analysis of relative NBD-PG levels in whole cells (H) and isolated mitochondria (I) of vector control and MFN2 KO cells.

Data are expressed as mean ± SD; *$p < 0.05$, **$p < 0.01$, and ***$p < 0.001$ by one-way ANOVA or Student's t test. ns, non-significance.

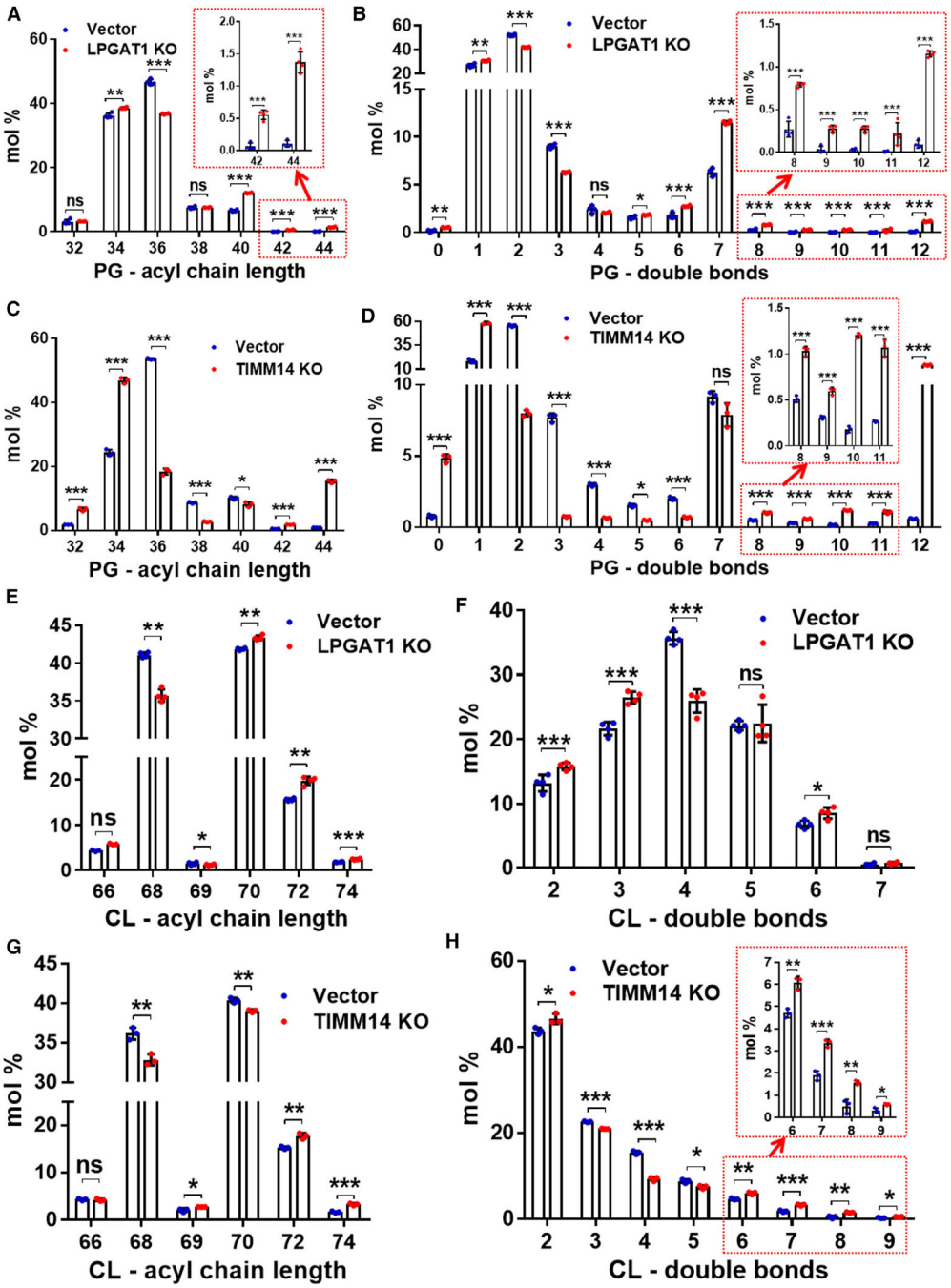

Figure 7. Loss of LPGAT1 or TIMM14 causes similar alterations in PG and CL acyl compositions

Lipidomic analysis acyl chain compositions of PG and CL in C2C12 vector control, LPGAT1 KO, and TIMM14 KO cells by mass spectrometry.

(A and B) The relative levels of PG with different acyl chain lengths (A) and double bonds (B) in vector control and LPGAT1-deficient cells. n = 4.

(C and D) The relative levels of PG with different acyl chain lengths (C) and double bonds (D) in vector control and TIMM14-deficient cells. n = 3.

(E and F) The relative levels of CL with different acyl chain lengths (E) and double bonds (F) in vector control and LPGAT1-deficient cells. n = 4.
(G and H) The relative levels of CL with different acyl chain lengths (G) and double bonds (H) in vector control and TIMM14-deficient cells. n = 3.
Data are expressed as mean ± SD; *$p < 0.05$, **$p < 0.01$, and ***$p < 0.001$. ns, non-significant, by Student's t test. Boxes highlight enrichment of polyunsaturated fatty acyl chains in PG of LPGAT1- and TIMM14-deficient cells.

KEY RESOURCES TABLE

REAGENT or RESOURCE	SOURCE	IDENTIFIER
Antibodies		
Rabbit polyclonal anti-PHB1	Cell Signaling Technology	Cat#2426S; RRID:AB_823689
Rabbit monoclonal anti-PHB2 (Clone E1Z5A)	Cell Signaling Technology	Cat#14085S; RRID:AB_2798387
Mouse monoclonal anti-β-Actin (Clone AC-74)	Sigma-Aldrich	Cat#A2228; RRID:AB_476697
Mouse monoclonal anti-FLAG (Clone M2)	Sigma-Aldrich	Cat#F3165; RRID:AB_259529
Rabbit polyclonal anti-DNAJC19	Proteintech	Cat#12096–1-AP; RRID:AB_2094914
Rabbit polyclonal anti-TIMM23	Proteintech	Cat#11123–1-AP; RRID:AB_615045
Rabbit polyclonal anti-TIMM44	Proteintech	Cat#13859–1-AP; RRID:AB_2204679
Rabbit polyclonal anti-TIMM50	Proteintech	Cat#22229–1-AP; RRID:AB_2879039
Rabbit polyclonal anti-AFG3L2	Proteintech	Cat#14631–1-AP; RRID:AB_2242420
Rabbit polyclonal anti-MFN2	Proteintech	Cat#12186–1-AP; RRID:AB_2266320
Mouse polyclonal anti-LPGAT1	This Paper	N/A
Goat anti-Rabbit IgG (H + L) Secondary Antibody, HRP	Thermo Fisher Scientific	Cat#31463; RRID:AB_ 228333
Goat anti-Mouse IgG (H + L) Secondary Antibody, HRP	Thermo Fisher Scientific	Cat#31430; RRID:AB_228307
Bacterial and virus strains		
DH-5α	Thermo Fisher Scientific	Cat# 18265017
Chemicals, peptides, and recombinant proteins		
Collagenase, Type IV	Thermo Fisher Scientific	Cat#17104019
Hoechst 33342	Invitrogen	Cat#62249
MitoTracker Red CMXRos	Invitrogen	Cat#M7512
Oligomycin	Sigma-Aldrich	Cat#O4876; CAS:1404–19-9
Carbonyl cyanide 4-(trifluoromethoxy) phenylhydrazone (FCCP)	Sigma-Aldrich	Cat#C2920; CAS:370–86-5
Rotenone	Sigma-Aldrich	Cat#R8875; CAS:83–79-4
Antimycin A from *Streptomyces* sp	Sigma-Aldrich	Cat#A8674; CAS:1397–94-0
[N-[(7-nitro-2–1,3-benzoxadiazol-4-yl)-methyl]amino] palmitoyl Coenzyme A (16-NBD-16:0 Coenzyme A)	Avanti Polar Lipids	Cat#810705; CAS:1367862–09-6
1-oleoyl-2-hydroxy-*sn*-glycero-3-phospho- (1'-rac-glycerol) (18:1 LPG)	Avanti Polar Lipids	Cat#858125; CAS:326495–24-3
1-oleoyl-2-hydroxy-*sn*-glycero-3-phosphocholine (18:1 LPC)	Avanti Polar Lipids	Cat#845875; CAS:19420–56-5
1-oleoyl-2-hydroxy-*sn*-glycero-3-phosphoethanolamine (18:1 LPE)	Avanti Polar Lipids	Cat#846725; CAS:89576–29-4
monolysocardiolipin (Heart, Bovine) (MLCL)	Avanti Polar Lipids	Cat#850081; CAS:383907–65-1
1-oleoyl-2-{12-[(7-nitro-2–1,3-benzoxadiazol-4-yl)amino]dodecanoyl}-*sn*-glycero-3-[phospho-rac-(1-glycerol)] (18:1–12:0 NBD-PG)	Avanti Polar Lipids	Cat#810166; CAS:474942–88-6
Viafect transfection reagent	Promega	Cat#E4982
X-tremeGENE™ HP DNA transfection reagent	Sigma	Cat# XTGHP-RO
Lipofectamine RNAiMAX transfection reagent	Invitrogen	Cat# 13778150

REAGENT or RESOURCE	SOURCE	IDENTIFIER
Puromycin dihydrochloride	APExBIO	Cat#B7587; CAS:58–58-2
DMEM	Sigma	Cat#D5796
0.25% Trypsin-EDTA	GIBCO	Cat#25200–072
Pen Strep	GIBCO	Cat#15140–122
Fetal Bovine Serum	Atlanta Biologicals	Cat#S11550H
ProteinA/G PLUS-Agrose	Santa Cruz	Cat#sc-2003
TRIzol Reagent	Invitrogen	Cat#15596018
DNase I	Sigma	Cat#10104159001
Hyaluronidase	Sigma	Cat#H3506
Wheat germ agglutinin	Thermo Fisher Scientific	Cat#W11261
EDTA-free protease inhibitors cocktail	Sigma	Cat#11873580001
Chloroform	Sigma	Cat#319988
Methanol	Sigma	Cat#179337
Critical commercial assays		
Alanine aminotransferase Assay Kit	Nanjing Jiancheng Bioengineering Institute	Cat#C009–2-1
Aspartate aminotransferase Assay Kit	Nanjing Jiancheng Bioengineering Institute	Cat#C010–2-1
Total bilirubin (T-BIL) Assay Kit	Nanjing Jiancheng Bioengineering Institute	Cat#C019–1-1
Blood Ammonia Assay Kit	Nanjing Jiancheng Bioengineering Institute	Cat#A086–1-1
Urea Assay Kit	Nanjing Jiancheng Bioengineering Institute	Cat#C013–2-1
Lactic Acid Assay Kit	Nanjing Jiancheng Bioengineering Institute	Cat#A019–2-1
EnzyChrom Pyruvate Assay Kit	BioAssay Systems	Cat#EPYR-100
Hematoxylin-Eosin (HE) Stain Kit	SolarBio	Cat#G1120
Masson's Trichrome Stain Kit	SolarBio	Cat#G1340
Reactive Oxygen Species (ROS) Assay Kit	Beyotime Biotechnology	Cat#S0033S
Pierce BCA Protein Assay Kits	Thermo Fisher Scientific	Cat#23225
Experimental models: Cell lines		
C2C12	ATCC	Cat#CRL-1772; RRID:CVCL_0188
HEK293T	ATCC	Cat#CRL-11268; RRID:CVCL 192
Primary mouse embryonic fibroblasts	This paper	N/A
Primary hepatocytes	This paper	N/A
Experimental models: Organisms/strains		
Mouse: C57BL/6J *Lpgat1*$^{-/-}$	This paper	N/A
Mouse: C57BL/6J	The Jackson Laboratory	Strain #:000664; RRID:IMSR_JAX:000664
Oligonucleotides		

REAGENT or RESOURCE	SOURCE	IDENTIFIER
Primers for qPCR	Table S1	N/A
Recombinant DNA		
Plasmid: pcDNA3.1(+)-FLAG-LPGAT1	This paper	N/A
Plasmid: mito-BFP	Addgene	Plasmid #49151; RRID:Addgene_4915
Plasmid: dsRed2-ER5	Addgene	Plasmid #55836; RRID:Addgene_55836
Plasmid: pBABE-puro	Addgene	Plasmid #1764; RRID:Addgene_1764
Human MFN2 siRNA	Sigma	Cat#SASI_Hs02_00330014
Control siRNA	Sigma	Cat#SIC001
Mouse LPGAT1 CRISPR/Cas9 KO Plasmid	Santa Cruz	#sc-432665
Mouse LPGAT1 HDR Plasmid	Santa Cruz	#sc-432665-HDR
Mouse TIMM14 CRISPR/Cas9 KO Plasmid	Santa Cruz	#sc-426704
Mouse TIMM14 HDR Plasmid	Santa Cruz	#sc-426704-HDR
Mouse MFN2/Mitofusin 2 CRISPR/Cas9 KO Plasmid	Santa Cruz	#sc-431291
Mouse MFN2/Mitofusin 2 HDR Plasmid	Santa Cruz	#sc-431291-HDR
Software and algorithms		
ImageJ	National Institutes of Health	https://ImageJ.net/ij/index.html
Xcalibur	Thermo Scientific	https://www.thermofisher.cn/order/catalog/product/OPTON-30965?SID=srch-srp-OPTON-30965
Seahorse Wave Controller	Agilent	https://www.agilent.com.cn/zh-cn/product/cell-analysis/real-time-cell-metabolic-analysis/xf-software/seahorse-wave-controller-software-2-4-2-740903
GraphPad Prism	GraphPad, Inc	https://www.graphpad.com/scientific-software/prism/
Other		
TLC plates	Sigma	60805
SpectraMax M2 microplate reader	Molecular Devices	M2
Seahorse XF96 analyzer	Agilent	XF96
Vevo 2100 Imaging System	Visual Sonics	Vevo 2100